POLITECNICO DI TORINO

Master Degree course in Physics of Complex Systems

Master Degree Thesis

Totally asymmetric exclusion process connected to weakly-coupled finite reservoirs

Politecnico di Torino

Supervisors:
Alessandro Pelizzola
Marco Pretti

Candidate:
Francesco Ferro

Academic Year 2023-2024

Contents

Chapter 1

Introduction

Out of the infinitely many physical phenomena that permeate the universe, out-of-equilibrium processes play a very special and pervasive role. In fact, at any given moment, anyone is surrounded by out-of-equilibrium processes (e.g. traffic flow, electrical or heat transport) and is even host for some of them (think of biological transport inside our bodies). Among the many instances in which out-of-equilibrium physics arises, a very important category of interesting problems is that of transport phenomena. Be it in the realm of biology or rush hour traffic, a lot of things have to be transported to make life and the world work as we know it. In the present thesis, we use statistical mechanics to deal with a model developed in the context of biological transport, with the purpose of finding information on its steady states, i.e. the situations for which its macroscopic behaviour does not change over time. In the domain of non-equilibrium statistical mechanics, there is no well-established theory to study, therefore, some models have been proposed as a means of capturing the relevant physical properties of multi-particle out-of-equilibrium systems. One of these tools, called TASEP, is the paradigmatic one used especially as a toy model for the one-dimensional driven motion of a set of particles. TASEP stands for 'Totally Asymmetric Simple Exclusion Process', and is defined as a one-dimensional lattice consisting of L sites governed by a specific set of rules. In its simplest configuration, the fundamental features of the model are:

- particles are only as big as one site,
- sites can be either empty or occupied by only one particle,
- particles can hop only to their first neighbouring site and only in a set direction (for example, rightward),
- only one particle at a time moves.

As previously stated, there is a biological background behind the TASEP. In fact, in 1968, Macdonald et al. [1] proposed it as a model for the so-called 'translation'

part of protein biosynthesis, consisting of the motion of ribosomes along mRNA. Protein biosynthesis is the process in a cell in which a genetic code encrypted in DNA is translated into the production of proteins, biomolecules that have a huge variety of roles inside living things. This process starts with a 'transcription' phase where a messenger RNA (mRNA) is created from DNA and later ejected out of the cell nucleus into the cytoplasm, where the 'translation' phase occurs (as shown in fig. 1.1).

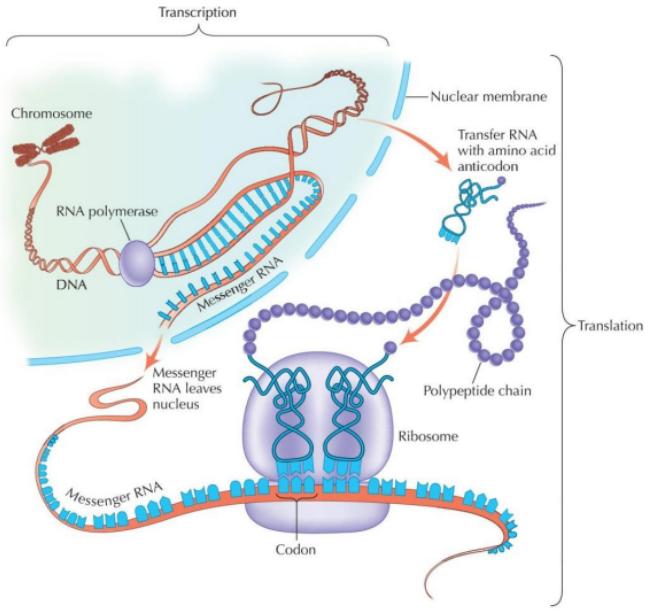

Figure 1.1: Visual representation of protein synthesis. The picture was taken from [2].

During this phase, a set of ribosomes binds to one mRNA molecule at a specific location called starting codon[1]. Then, these ribosomes move along the mRNA, in a set direction, translating each codon into a specific amino acid. The biochemical mechanics that govern ribosomes' movement are the ones responsible for driving the system out of equilibrium. We can see that the main features of ribosome kinetics justify the modelling via TASEP[2]:

- the movement of ribosomes on the mRNA molecule looks like the motion of particles on a one-dimensional track;
- the ribosomes couple with codons and move from one codon to the next,

[1]We remind that a codon is a group of three consecutive nucleotides.

[2]Some features of the kinetics are not captured in the modelling because of the unitary particle size and the uniform hopping rates in the TASEP.

which can be viewed as the one-dimensional track having a lattice structure where codons are the sites;

- there cannot be two ribosomes coupled to the same codon at once, thus a 'simple exclusion' rule is satisfied.

After this first instance, the TASEP acquired, for non-equilibrium processes, a role comparable to that of the Ising model for equilibrium processes. Therefore, it has been implemented as a modelling tool in many different fields, both biological (e.g. to represent the movement of myosin or the transport of cellular material performed by kinesin and dynein) and not (vehicular traffic phenomena, among others). Of course, when dealing with difficult and multifaceted problems, there is always more complexity to be dealt with. The TASEP, as we described it, is a very simplified way to model the basic behaviour of certain systems. However, a deeper understanding of the complicated dynamics of a particular system under investigation can be reached by modifying the features of the 'simple' TASEP and introducing some new ones. For example, one often deals with biological or other physical systems in which the resources are limited. In the context of protein synthesis, the finite resources correspond to a finite number of ribosomes available for translation. This prompts the study of lattice models that are closed. In the literature, many of such systems have been investigated, a lot of them being idealized ones, not necessarily associated with a specific physical system [3–7]. This area of research is still active and in this thesis work we aim at investigating one of such models. We will analyse a closed system composed of a TASEP inserted between two reservoirs that interact with each other by exchanging particles at some given fixed rates. Naturally, this imposes a conservation of the overall number of particles. For this particular system, an exact solution is not known. So, we will utilise both approximate semi-analytical methods and computer simulations to find some results about the steady-state behaviour we are interested in.

The thesis is organised as follows: In Chapter 2 we introduce the main results and methods used to tackle the study of 'simple' TASEP (sections 2.1, 2.2) and specify the features of the specific system we consider in this thesis (section 2.3). In Chapter 3 we first describe how to build up a numerical algorithm for simulating our problem using the kinetic Monte Carlo method (section 3.1). Then, we proceed to write the governing equations of the system under a Mean Field approximation and we show how they can guide us in understanding the steady states of the model (sections 3.2, 3.3). We use the name 'constraints analysis' for section 3.3 because, as it will be shown later, we will use some specific constraints on the reservoirs' populations to extract information on the admitted phases for the system at stationarity. In Chapter 4 we thoroughly report the results obtained by the previously presented methods. In Chapter 5 we briefly summarize the findings of this thesis work and mention possible future developments.

Chapter 2

Models

As stated in the introduction, the TASEP is a model defined, in its simplest form, on a one-dimensional lattice composed of L sites in which particles can move only from a certain site to its right adjacent one, as long as the latter is empty, with unit rate. Given the length L of the lattice, it is customary to label the sites, starting from the left border, with $i = 1, \dots L$, and introduce the random variables $n_i^t = 0{,}1$ which relay the information concerning the occupation of a site i at a certain time, e.g. if the site i is empty (full) at time t, then $n_i^t = 0(1)$. For the effective study of the model, the local densities of particles are introduced $\rho_i^t = \langle n_i^t \rangle$. Here, the notation $\langle . \rangle$ means 'expectation value' and stands for the ensemble average over all the possible outcomes of the stochastic process at any time.

From this simple setup, one can introduce a variety of complications and obtain a plethora of interesting models with different behaviours. Among the most famous ones, are the 'Partially Asymmetric Simple Exclusion Processes' in which particles can jump in both directions (with different rates)[8], the TASEP with Langmuir kinetics, in which attachment and detachment of particles can occur at any site [9], the one with particles occupying more than one lattice site [10] or with site-wise disorder [11] and many others.

However, for any model or complication one wants to tackle, and even in its most simple version, the TASEP has an important degree of freedom that one needs to specify, the boundary conditions. The first and most important ones considered in the literature are periodic (PBC) and open (OBC) boundary conditions. As explained in the introduction, this thesis work will focus on a TASEP (related to the OBC case) connected to two weakly coupled reservoirs (more details later). Therefore, in this chapter, we will first briefly analyze the paradigmatic case of PBC, which will serve as a first introduction to some machinery and way of thinking needed in future sections, then we are going to introduce the main features of the model with OBC and in the end we will concisely show how considering two coupled reservoirs modifies the picture. A detailed and extensive analysis will follow in the next chapters.

2.1 TASEP with periodic boundary conditions

For the TASEP, the requirement of periodic boundary conditions makes it so that our one-dimensional lattice takes the shape of a ring where site L is connected to site 1 and a particle can hop from the former to the latter (provided the latter is empty). The following figure should show clearly what we mean.

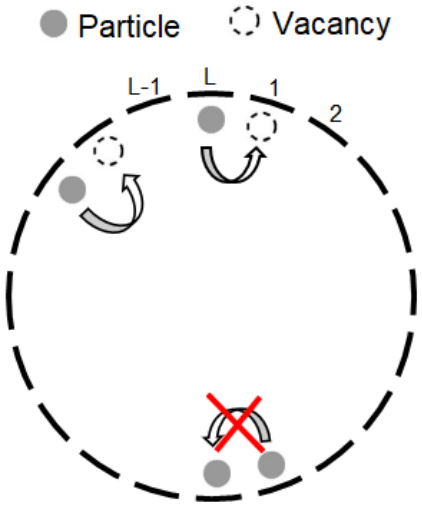

Figure 2.1: Visual representation of a simple TASEP with PBC.

As a consequence of the topology of the system, particles cannot enter or exit the ring and the total number of particles present in the initial state will not vary. This number therefore will be conserved during the dynamics. We denote this by writing

$$N = \sum_{i=1}^{L} n_i^t = \sum_{i=1}^{L} n_i^0. \tag{2.1}$$

Now let us delve deeper into the dynamics of the system. Let us take a certain configuration of the system with N particles and denote by k the number of clusters of adjacent particles present at a certain time t. The rules of the motion prevent from moving any particle that is not the rightmost one of a cluster. Therefore there are exactly k possible transitions to a different configuration. For the same consideration, there are also exactly k configurations from which the present state can be reached through a transition. This reasoning allows us to draw the conclusion that the stationary state probability is a non-zero constant for every configuration that has precisely N particles and is zero otherwise. We can sum up this information by writing:

$$P(n^t) = const \cdot \delta_{\sum_{i=1}^{L} n_i^t, N}. \tag{2.2}$$

Now to find this constant one just needs to use normalisation. In fact, having N particles in a lattice of L sites means that the ways in which one can distribute those N particles into the L sites are given by the simple combinatorial result $\binom{L}{N} = \frac{L!}{N!(L-N)!}$. Therefore

$$P(n^t) = \frac{N!(L-N)!}{L!} \cdot \delta_{\sum_{i=1}^{L} n_i^t, N}. \tag{2.3}$$

Following the previous considerations, it ensues that the probability flux into and out of a certain configuration at time t with k clusters will be k times the previously stated constant, and the stationarity condition given by the master equation of the process is satisfied:

$$\frac{d}{dt}P(n^t) = k\frac{N!(L-N)!}{L!} - k\frac{N!(L-N)!}{L!} = 0 \tag{2.4}$$

Armed with these results one can derive stationary state densities and correlations. Firstly, the probability of having a particle at a certain site i can be obtained with the easy combinatorial consideration[1]

$$\rho = \langle n_i \rangle = P(n_i = 1) = \frac{\binom{L-1}{N-1}}{\binom{L}{N}} = \frac{\frac{(L-1)!}{(N-1)!(L-N))!}}{\frac{L!}{N!(L-N)!}} = \frac{\frac{(L-1)!}{(N-1)!(L-N))!}}{\frac{L(L-1)!}{N(N-1)!(L-N)!}} = \frac{N}{L} \tag{2.5}$$

and one can clearly see that this stationary density is independent of the specific lattice site considered. For the correlations, one can see an emerging pattern. Let us start with the two-point correlation, which can also be restated as the probability of finding a particle at $j \neq i$, given that there is a particle at i. We can write

$$\langle n_i n_j \rangle = P(n_i = 1, n_j = 1) = P(n_j = 1 | n_i = 1)P(n_i = 1) = \frac{N(N-1)}{L(L-1)} \tag{2.6}$$

using the same kind of reasoning as before. The three-points correlation will have form $\langle n_i n_j n_k \rangle = \frac{N(N-1)(N-2)}{L(L-1)(L-2)}$ and the general form for any order emerges recursively as

$$\underbrace{\langle n_i n_j \dots n_k \rangle}_{R \text{ sites}} = \prod_{m=0}^{R-1} \frac{(N-m)}{(L-m)}. \tag{2.7}$$

Now the remarkable feature of this result is that, by taking the thermodynamic limit, i.e. having $N, L \to +\infty$ such that $\frac{N}{L}$ remains constant, the correlations and the stationary state probability factor into products of single node marginals

$$\langle n_i n_j \rangle = \rho^2, \qquad \langle n_i n_j n_k \rangle = \rho^3, \dots, \tag{2.8}$$

[1]The probability of having a particle in site i is equal to all the ways in which the $N-1$ remaining particles can be distributed in the $L-1$ sites left divided by all the possible ways to distribute N particles in L sites.

thus making a mean field assumption exact. In this stationary state, the particle current can be written as

$$J(\rho) = \langle n_i(1 - n_{i+1}) \rangle = \rho(1 - \rho). \tag{2.9}$$

This current describes how fast is the motion of particles in the TASEP with respect to the particle density in the thermodynamic limit. The plot J vs ρ is known as fundamental diagram:

Figure 2.2: Fundamental diagram of TASEP with PBC.

We can see that $J(\rho)$ is zero for particle density 0 and 1, corresponding to the lattice being totally empty or totally full, and it is maximal ($J = \frac{1}{4}$) for the optimal density $\rho = \frac{1}{2}$. In this introduction, we were only concerned with the stationary state of the system. A full non-stationary solution was found in 2003 by Priezzhev [12].

2.2 TASEP with open boundary conditions

In this subsection, we go over the main features and the important results for the TASEP with OBC, with unitary and uniform transition rates. In its simplest form, we consider particles to be injected at the first site of the TASEP (given that it is empty) with constant rate α and extracted from the last site L (provided it is occupied) with rate β. It is interesting to notice that a completely equivalent description can arise assuming that the TASEP is in contact with two infinite reservoirs of fixed densities α,$1 - \beta$ which respectively inject and extract particles at unit rate. A schematic representation of the whole system is given in figure 2.3.

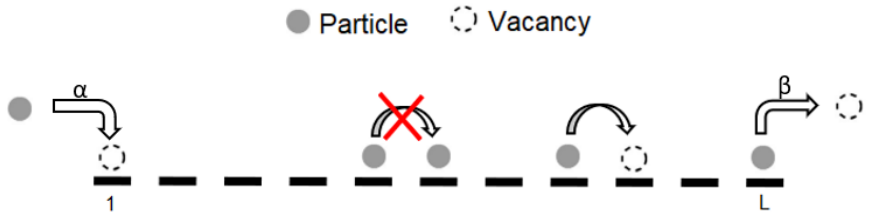

Figure 2.3: TASEP with open boundary conditions, injection rate α and ejection rate β.

The fascinating feature of this system is that the macroscopic behaviour of the steady state is strictly determined by the parameters at the boundaries. In fact, by fine-tuning the values of α and β one can induce a modification of the stationary density profile that can be described with the language of phase transitions. We can call α and β the control parameters and the bulk (uniform) density ρ the order parameter. Depending on the values of the control parameters, the stationary state of the system can be in three different phases, characterised by different behaviours of the order parameter:

- With $\alpha < \beta$ and $\alpha < \frac{1}{2}$ the bulk density is $\rho = \alpha < \frac{1}{2}$ and one describes the TASEP as being in a Low Density (LD) Phase.
- With $\beta < \alpha$ and $\beta < \frac{1}{2}$ the bulk density is $\rho = 1 - \beta > \frac{1}{2}$ and one describes the TASEP as being in a High Density (HD) Phase.
- With $\alpha, \beta > \frac{1}{2}$ the bulk density is $\rho = \frac{1}{2}$ and one describes the TASEP as being in a Maximal Current (MC) Phase

As previously stated, it is interesting to notice that the value of the bulk density ρ, describing the system at a macroscopic level, is the result of the behaviour of the TASEP at the boundaries. While this is unusual, it is intuitively clear how, in the specific case at hand, the TASEP can be in a low density phase (so there are, on average, not many particles inside at any given moment) when particles exit faster than they enter ($\alpha < \beta$) and, vice versa, it can be in a high density phase when particle enter faster than they exit. The maximal current phase is maybe less transparent but it can be described as the situation for which, as its name suggests, the boundary parameters are permitting the 'fastest possible passage' of particles going through the TASEP. It is also important to remark that the boundary between HD and LD phases is delimited by the so-called coexistence line, namely for $\alpha = \beta$ with $\alpha, \beta < \frac{1}{2}$. On this line, the system shows a linear density profile that connects low local densities close to the injection border to high local densities close to the

ejection border. In this situation, see fig. 2.5, one obtains a domain wall (or shock) profile via mean field approximation. The exact solution is recovered considering that in the limit $L \to +\infty$ the domain wall can be anywhere and an infinite number of solutions appear, whose average gives the linear profile mentioned before. We thus say, for the coexistence line, that there is a 'delocalised' domain wall. Lastly, one can notice that the transition between low and high density phases through the coexistence line is characterised by a jump in the bulk density. This transition is named discontinuous (or 1^{st} order). Conversely, the transitions between a high (low) density phase and the maximal current phase present a smooth transition in ρ. This is said to be a continuous (or 2^{nd} order) phase transition.

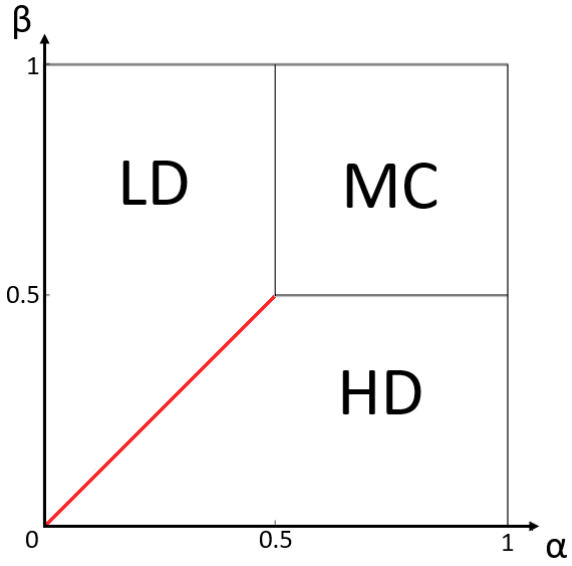

Figure 2.4: Phase diagram for TASEP with open boundary conditions and unitary hopping rates.

We extensively listed the characteristics of this simple model, let us quickly go over how one can find these results. The simplest idea (which we will also use in future sections for the extended model under study in this thesis work) is to consider a Mean Field approximation where, motivated by the promising results of the TASEP with PBC, one assumes that at each time t the joint probability distribution factors into single-site marginals. This approximation allows one to write the local currents as

$$J_i^t = P_i^t(1,0) = \rho_i^t(1-\rho_{i+1}^t) \qquad i=1,\dots L-1 \tag{2.10}$$

and the continuity equations describing the time evolution of the local densities as

$$\dot{\rho}_i^t = J_{i-1}^t - J_i^t = \rho_{i-1}^t(1-\rho_i^t) - \rho_i^t(1-\rho_{i+1}^t) \qquad i=2,\dots L-1 \tag{2.11}$$

with boundary conditions:

$$\dot{\rho}_1^t = \alpha(1-\rho_1^t) - \rho_1^t(1-\rho_2^t) \tag{2.12}$$
$$\dot{\rho}_L^t = \rho_{L-1}^t(1-\rho_L^t) - \beta\rho_L^t \tag{2.13}$$

In principle, we could numerically solve these equations and look for solutions at a sufficiently long time for which a stationary state is reached. Otherwise, given that we are only looking for information on the stationary state of the model, we can also equate to zero the right hand sides of the previous equations. What we obtain is a set of L equations in L unknowns to be solved at given values of the parameters α and β. Whatever the path one decides to take, for the TASEP with OBC the mean field approximation yields a phase diagram containing all the correct phases and transitions and satisfying results for the bulk densities. However, the full density profiles obtained in Mean field turn out to be incorrect, especially near the boundaries for HD, LD and MC phases, and as a whole on the coexistence line, as shown in the figure below.

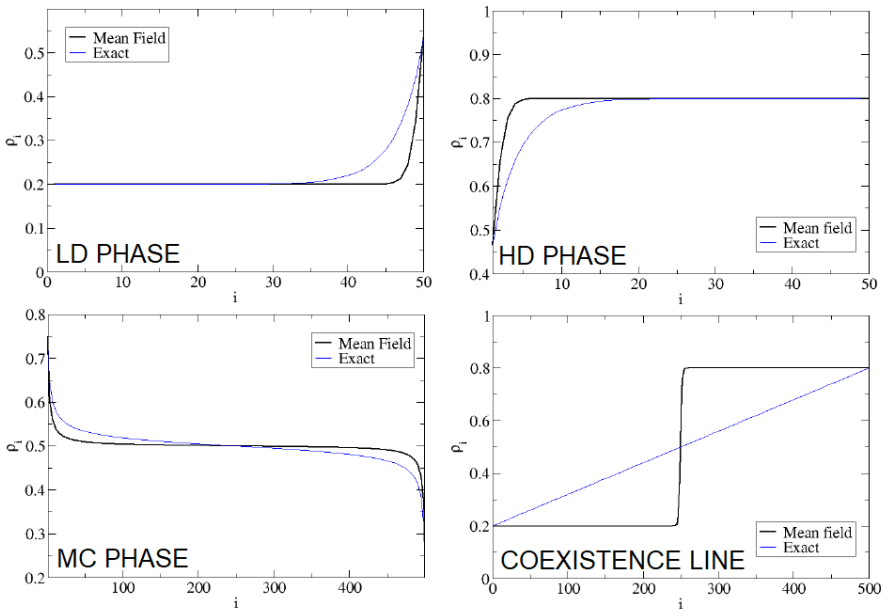

Figure 2.5: Comparison of full density profiles computed exactly and through Mean Field approximation for the TASEP with OBC.

The exact solution for this model was found in the early 1990s by Derrida et al. [13–16]. For a generic extension of the model, like the one we are analysing in this thesis, there is no established method to use and one needs to start tackling the problem in different directions. One of the first ideas that comes to mind is trying

a Mean Field approximation, which we will in fact use. For this reason, we have briefly presented it here for the case of a simple TASEP OBC. Another method could be that of using computer simulations to study the system, for example via Monte Carlo Method. We will also make use of this tool, therefore, to close this section, we want to convey its power by showing below an example of the full density profile of a simple TASEP with OBC, $L = 50$, $\alpha = 0.2$, $\beta = 0.3$ obtained via Mean Field approximation and via Monte Carlo simulation and then comparing them with the exact result. One can clearly see in the figure that the full profile obtained via simulation perfectly matches the exact one.

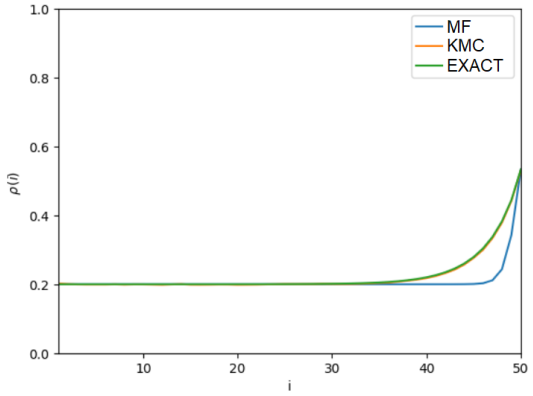

Figure 2.6: Comparison of a full density profile computed exactly, through Mean Field approximation and via Kinetic Monte Carlo simulation.

2.3 TASEP connected to two coupled reservoirs

We can now describe the model on which we focus in this thesis. This is, as anticipated before, an extension of the system presented in the previous section. We know that a complete description of the TASEP with OBC is obtained by considering the lattice in contact with two non-interacting and infinite reservoirs with fixed densities. In the present work, we will focus on a system for which the injection and extraction mechanisms of the TASEP are linked to two interacting reservoirs of finite sizes [17]. A sketch of the model is shown in figure 2.7.

The system is made up of a one-dimensional TASEP of L sites connected to two reservoirs R_1 and R_2. The particles in the first reservoir can enter the TASEP, provided that the first site is empty. Then, inside the lattice, the particles follow the usual rules of hopping only one place rightward, with unitary rate and only if the next site is empty. When a particle reaches the last site, it can leave by entering the second reservoir. The reservoirs can be described as points without spatial extent or internal dynamics. Moreover, the reservoirs can exchange particles between

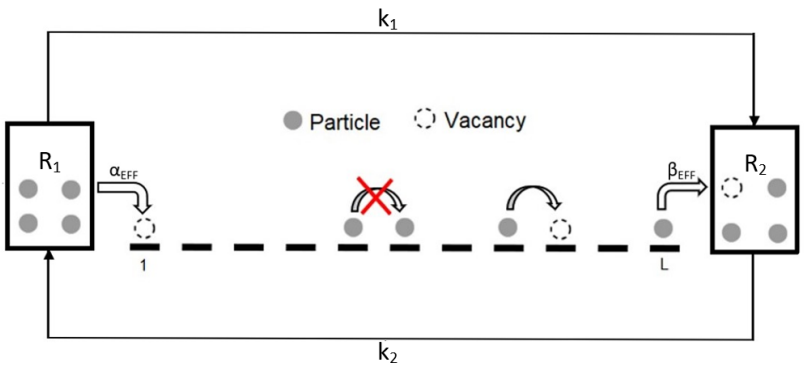

Figure 2.7: Schematic of the system.

them directly. This is done in order to ensure a steady current in the system since the flow through the TASEP is unidirectional and thus would stop shortly after the depletion of particles in R_1. To model this phenomenon, the instantaneous diffusion rates k_1 and k_2 are defined. With this particle exchange mechanism in place, one easily understands that the global number of particles in the system is a conserved quantity. This conservation rule can be written as

$$N_{TOT} = N_1 + N_2 + N_T \tag{2.14}$$

Where N_{TOT} is the global number of particles in the system, N_1 and N_2 are the number of particles in R_1 and R_2, and N_T denotes the number of particles in the TASEP ($N_T = \sum_{i=1}^{L} n_i$, with n_i the occupation number of site i). We will further require that the reservoirs' capacities be bounded. More precisely, the model is defined such that $N_2 \leq L$ and $N_1 \leq N_{TOT}$. Let us now be more precise about the interactions among the TASEP and the reservoirs. We are used to having two fixed parameters α and β that regulate injection and extraction. In the current model, we do not want to have fixed but dynamic rates. We would like to see that the injection to the TASEP increases its rate the more particles are present in R_1 and that the extraction from the TASEP lowers its rate the more particles are in R_2. To achieve the wanted behaviour, we introduce, as done in [17], the effective reservoir population-dependent injection and extraction parameters:

$$\alpha_{EFF} = \alpha\frac{N_1}{L} \qquad \beta_{EFF} = \beta(1 - \frac{N_2}{L}) \tag{2.15}$$

Here, α and β are control parameters that can take any positive value. These control parameters are multiplied by suitably chosen functions of N_1 and N_2 that are, respectively, monotonically increasing and decreasing non-negative functions, that permit to respect the requirements stated before on the exchange flows we want

the TASEP to have[2]. Moreover, a parameter called the filling factor is defined as $\mu = \frac{N_{TOT}}{L}$. This parameter gives us information on how populated the total system is, in relation to the size of the TASEP. In the end, the model has five parameters $(\alpha, \beta, \mu, k_1, k_2)$ which control its behaviour. Lastly, as the title of this thesis suggests, we remind that in this work we will focus our investigation of the present system in a regime that corresponds to having the two reservoirs weakly coupled. We will be more precise about what this entails in the next chapter.

[2]In principle, one could choose more complicated functions that respect the same physical and mathematical requirements. Nevertheless, these simple choices are sufficient to observe some interesting behaviour in the system.

Chapter 3

Methods

In this work, we used two main techniques. Guided in spirit by the efficacy of mean field approximation in correctly predicting the stationary states of the TASEP with both PBC and OBC and by the extraordinary insights and power of simulation methods, we use a mixture of both analytical and numerical tools to understand the system under study and to interpret its behaviour. In the following sections, we are going to describe in detail how.

3.1 Kinetic Monte Carlo

This technique consists of implementing an algorithm, first developed by Gillespie in the late seventies [18] (therefore it is also known as Gillespie algorithm), to efficiently simulate continuous time Markov processes. The main feature of this algorithm, which is also what prompted us to utilise it, is that it is a rejection-free Monte Carlo method. In fact, during the simulation, the program draws at random what the next transition will be and when it will occur, instead of trying and accepting/rejecting a transition at each temporal step. Thus, this generation method is 100% efficient. Let us now briefly see how this method works. Consider a generic system under study at an initial time t in a predetermined initial configuration. If one lets the system naturally evolve, a new configuration will be reached at a certain time, where both the new configuration and the elapsed time are controlled by the stochastic dynamics of the system. Now, if one calls W_i the transition rate between two configurations (where i is an index spanning the set $\mathcal{S}$ of allowed transitions), then the probability that this transition occurs in the infinitesimal time interval $(t+\tau, t+\tau+d\tau)$, is

$$P(\tau, i)d\tau = P_0(\tau)d\tau W_i \tag{3.1}$$

with $P_0(\tau)$ being the probability that no transition occurs in the interval $(t, t+\tau)$, where t is the time at which the last transition occurred. $P_0(\tau)$ can be computed by dividing the interval $(t, t+\tau)$ in m sub-intervals $\Delta\tau = \frac{\tau}{m}$, considering no transition

should happen in all these sub-intervals, and taking the limit $m \to +\infty$; giving

$$P_0(\tau) = \left(1 - \frac{\tau}{m}\sum_{l\in\mathcal{S}} W_l\right)^m \to e^{-\tau\sum_{l\in\mathcal{S}} W_l}. \tag{3.2}$$

This result means that

$$P(\tau, i) = W_i e^{-\tau\sum_{l\in\mathcal{S}} W_l}. \tag{3.3}$$

Now, to specify what transition will occur and when, one needs to sample a pair (τ, k) from a set described by $P(\tau, k)$. Gillespie shows that this can be achieved by generating two random numbers ξ_1, ξ_2 from a unit-interval uniform distribution and then by plugging them into the formulas below:

$$\tau = -\frac{1}{\sum_{l\in\mathcal{S}} W_l}\ln\xi_1 \tag{3.4}$$

$$\sum_{l=0}^{k-1} W_l < \xi_2 \sum_{l\in\mathcal{S}} W_l \leq \sum_{l=0}^{k} W_l \tag{3.5}$$

The computer algorithm we have written to simulate the system under study consists of four main steps:

1. Set the values for the control parameters $(\alpha, \beta, \mu, k_1, k_2)$ and the lattice length L. Set the initial time $t = 0$ and define a maximum number of transitions T. Specify an initial configuration for the $N_{TOT} = \mu \cdot L$ particles in the system. We decided (after verifying it did not impact the results for the stationary states of the system[1]) this initial configuration to be one where all the particles are in the first reservoir R_1. Furthermore, assign the initial rates W_i.

2. Generate a random number ξ_1, use equation (3.4) to compute τ and update the total time elapsed to $t + \tau$.

3. Generate a second random number ξ_2 and choose the next transition k by checking the integer for which the inequalities in (3.5) are satisfied. Depending on the specific case, the transition could be the hopping of a particle into/inside of/out of the TASEP, or the transferring of a particle from one reservoir to the other.

4. Update the state of the system (which, in this case, corresponds to updating the variables associated with the occupation numbers of the sites/reservoirs involved in the hopping) and all the transition rates W_i referring to the neighbourhood of where the transition took place. Then, the algorithm goes back

[1] As one would expect, since the independence of the stationary states from the specific starting configuration is a general property of an irreducible Markov chain.

to step 2 and performs repeatedly this sequence 2-4 until the established number of transitions T is reached.

At the end of the simulation, we obtain the density of particles for each site of the TASEP and the occupation numbers of the reservoirs as an average over their respective occupation variables computed before each transition, weighted by the time elapsed before the successive transition:

$$\rho_i = \frac{1}{t_T - t_{T_0}} \sum_{j=T_0}^{T-1} n_i^{t_j} \cdot (t_{j+1} - t_j) \tag{3.6}$$

$$\langle N_1 \rangle = \frac{1}{t_T - t_{T_0}} \sum_{j=T_0}^{T-1} N_1^{t_j} \cdot (t_{j+1} - t_j) \tag{3.7}$$

$$\langle N_2 \rangle = \frac{1}{t_T - t_{T_0}} \sum_{j=T_0}^{T-1} N_2^{t_j} \cdot (t_{j+1} - t_j) \tag{3.8}$$

As one usually does in these simulations, the sum starts not from the first transition to avoid 'polluting' the measurements by the transient to the steady state. Therefore, we introduce a proper starting time T_0, set to $0.1T$ after testing.

Armed with this algorithm, we will use the simulations as a counterpart to our analytical approximations during our search for the stationary states of the system.

Before moving on, let us be a little more precise about the different transitions that can occur in the system and what they mean, in the algorithm, for the variables associated with the occupation numbers of sites/reservoirs and the rates W_i. Remember we are dealing with a lattice of L sites connected to two interacting reservoirs in the fashion of fig. 2.7. We called $n_i^t \in \{0,1\}$ the occupation numbers for the lattice sites and N_1^t, N_2^t the number of particles in the reservoir, at time t. We define $n^t = \{n_1^t, \ldots, n_L^t\}$, $n^{t+\tau} = \{n_1^{t+\tau}, \ldots, n_L^{t+\tau}\}$ the TASEP configurations at two successive times. We have $L + 3$ possible processes:

- a particle leaves R_1 and occupies the first site of the TASEP with rate $W^0_{n^{t+\tau},n^t} = \alpha_{EFF}(1 - n_1^t) = \alpha\frac{N_1^t}{L}(1 - n_1^t)$;
- $L - 1$ processes inside the TASEP in which a particle hops from one site to the next one, with rates $W^i_{n^{t+\tau},n^t} = n_i^t(1 - n_{i+1}^t)$, $1 \leq i \leq L - 1$;
- a particle exits the last site of the TASEP and enters R_2 with rate $W^L_{n^{t+\tau},n^t} = \beta_{EFF} n_L^t = \beta(1 - \frac{N_2^t}{L})n_L^t$;
- a particle leaves R_1 to go towards R_2 with rate $W^{L+1}_{n^{t+\tau},n^t} = k_1 N_1^t$;
- a particle leaves R_2 to go towards R_1 with rate $W^{L+2}_{n^{t+\tau},n^t} = k_2 N_2^t$.

As stated before, as a consequence of transitioning to a new state during the run of the algorithm, the system configuration and the rates of the transition processes (involving both the sites targeted by the hopping process and their neighbourhood) need to be updated. Let us give two examples:

- hopping process from a generic site i to site $i+1$ inside the TASEP. We had $n_i^t = 1$, $n_{i+1}^t = 0$ and we update these occupation numbers to $n_i^{t+\tau} = 0$, $n_{i+1}^{t+\tau} = 1$. The new rates are $W^{i-1}_{n^{t+\tau},n^t} = n_{i-1}^{t+\tau}$, $W^{i}_{n^{t+\tau},n^t} = 0$ and $W^{i+1}_{n^{t+\tau},n^t} = 1 - n_{i+2}^{t+\tau}$.

- ejection of a particle from node L to R_2. We had $n_L^t = 1$, N_2^t particles in R_2 and we update the configuration to have $n_L^{t+\tau} = 0$, and $N_2^{t+\tau} = N_2^t + 1$. The new rates are $W^{L-1}_{n^{t+\tau},n^t} = n_{L-1}^{t+\tau}$, $W^{L}_{n^{t+\tau},n^t} = 0$ and $W^{L+2}_{n^{t+\tau},n^t} = k_2 N_2^{t+\tau}$.

3.2 Mean Field

Having written an algorithm that allows us to tackle the system under investigation from the computational side, we would also like to obtain some analytical results. The first idea that comes to mind is to try to describe the system's behaviour by means of a mean field approximation. It should not surprise the fact that one can easily draw some similarities between the TASEP in our model and the one with OBC presented in section 2.2. In fact, to be more precise, the internal dynamics of the two models are exactly the same. What differs is the behaviour of the injection/ejection parameters, which in the present case are effective parameters not fixed in time, see equations (2.15). While we can expect this modification to change the steady state behaviour of the system, it should not modify the structure of the mean field equations for the TASEP. As we know, a mean field approach consists of neglecting correlations between particles. Its effects are the same as for the simpler OBC case on the local currents of our system, see equation (2.10). Thus, one could write the continuity equations describing the time evolution of the local densities as

$$\frac{d\rho_i^t}{dt} = J_{i-1}^t - J_i^t = \rho_{i-1}^t(1-\rho_i^t) - \rho_i^t(1-\rho_{i+1}^t) \quad \text{with } i = 2, \dots L-1 \tag{3.9}$$

with boundary conditions:

$$\begin{aligned} \frac{d\rho_1^t}{dt} &= \alpha_{EFF}^t(1-\rho_1^t) - \rho_1^t(1-\rho_2^t) = \alpha\frac{N_1^t}{L}(1-\rho_1^t) - \rho_1^t(1-\rho_2^t) \\ \frac{d\rho_L^t}{dt} &= \rho_{L-1}^t(1-\rho_L^t) - \beta_{EFF}^t\rho_L^t = \rho_{L-1}^t(1-\rho_L^t) - \beta(1-\frac{N_2^t}{L})\rho_L^t. \end{aligned} \tag{3.10}$$

This, however, is not a closed set of equations that allows us to analyse the system dynamics under the chosen approximation. We still lack equations for the number of

particles in the reservoirs that appear in equations (3.10). Considering the currents entering/exiting through the reservoirs, we can write:

$$\begin{aligned} \frac{dN_1^t}{dt} &= k_2 N_2^t - k_1 N_1^t - \alpha \frac{N_1^t}{L}(1-\rho_1^t) \\ \frac{dN_2^t}{dt} &= k_1 N_1^t - k_2 N_2^t + \beta(1-\frac{N_2^t}{L})\rho_L^t \end{aligned} \tag{3.11}$$

With these, we obtained a closed set of equations in the corresponding set of variables (ρ_i^t, N_1^t, N_2^t). We can now write a computer algorithm which solves the previous set of equations. This algorithm consists of four main steps:

1. Set the values for the control parameters $(\alpha, \beta, \mu, k_1, k_2)$ and the lattice length L. Set the initial time $t = 0$. Specify the initial values for the variables in the system. We decided to opt for an initialisation that corresponds to having all the particles in the first reservoir R_1 (this fixes $\rho_i^0 = 0, N_2^0 = 0, N_1^0 = N_{TOT} = \mu \cdot L$).

2. Compute the values for the local currents $J_i = \rho_i^t(1-\rho_{i+1}^t)$ for i=1,... $L-1$, $J_0 = \alpha\frac{N_1^t}{L}(1-\rho_1^t)$, $J_L = \beta(1-\frac{N_2^t}{L})\rho_L^t$.

3. Update the values for the local densities and the number of particles in the reservoirs after a time interval of duration Δ. To do so, use a discrete-time version of equations (3.9)-(3.10)-(3.11). To be clearer:

$$\rho_i^{t+\Delta} = \rho_i^t + \Delta(J_{i-1}^t - J_i^t) \tag{3.12}$$

   and same for N_1, N_2. Update the time as $t_{NEW} = t + \Delta$

4. Repeat steps 2-3 until convergence.

We still need to specify what convergence means for this algorithm. We want the system to be sufficiently close to the steady state. We then define a parameter $\zeta = |\frac{N_1^t}{L} - \frac{N_1^{t-\Delta}}{L}| + \sum_{i=1}^{L} \frac{|\rho_i^t - \rho_i^{t-\Delta}|}{L}$ that can quantify how close we are to stationarity and we stop the iterations of the algorithm when ζ is less than a certain value, that we specified to be 10^{-12}.

With this algorithm, we explore the space of control parameters to find information on the system. This will be done in the next chapter. However, we can give here some preliminary considerations. Following the ideas of [17] we can clearly see that the minimum value for the filling factor corresponds to not having particles in the system, so $\mu_{Min} = 0$ and the particle current inside the TASEP is obviously zero. We can then ask what is μ_{Max}, and how it depends on the other parameters of the system. We can imagine that $\mu = \mu_{Max}$ when the particle density in each site of the TASEP is its maximum allowed value, one. This means that the TASEP is

full and the density current must be zero since there is no way for particles to flow. Given that μ is maximum and the TASEP is full ($N_T = L$) we expect the reservoirs to be in the situation where they are at their maximum values. By looking at equations (3.11) at stationarity and considering the injection/ejection currents to be zero for the previous reasons, one gets that

$$\frac{N_{1_{Max}}}{N_{2_{Max}}} = \frac{k_2}{k_1} \rightarrow N_{1_{Max}} = \frac{k_2}{k_1} L \tag{3.13}$$

Taking the equation for particle number conservation (2.14) and inserting what we just found we get

$$\mu_{Max} = 2 + \frac{k_2}{k_1}, \tag{3.14}$$

and we see that the ratio $\frac{k_2}{k_1}$ is the one controlling the maximum value of the filling factor. We notice that, since said ratio lives in $(0, +\infty)$, $\mu_{Max} \in (2, +\infty)$. With these first considerations, we can see that k_1, k_2 will play a major role in defining the behaviour of the system. We will proceed, in the next chapter, to investigate the space of the control parameters α, β, for fixed k_1, k_2 and μ. Before moving on, though, we must add that two different regimes for the diffusion parameters $k_{1,2}$ can be identified. It should be apparent that, with μ fixed, N_1 and N_2 should increase with L, while the current inside the TASEP and at its boundaries should not. Then, looking at equations (3.11) one can see that, at stationarity, in the thermodynamic limit $L \rightarrow +\infty$, the injection and extraction currents become negligible with respect to the diffusion currents. Thus, it is asymptotically true that $k_1 N_1 = k_2 N_2$. This means that the population in the reservoirs is simply fixed by $\frac{k_2}{k_1}$ and we can say that diffusion dominates the system. This regime can be called the 'Strong Coupling' limit. A more interesting case would be to focus on a situation where the diffusion mechanism and particle hopping are comparable. This is ensured by using a 'mesoscopic' scaling for which $k_{1,2} = \frac{\kappa_{1,2}}{L}$, with $\kappa_1, \kappa_2 \sim O(1)$. This is the 'Weak Coupling' limit and will be, as stated before, the focus of this thesis. Standing on the ground of these considerations, we proceed in using the algorithm previously described to investigate the system. We find correct information on its steady states, which are also supported by the simulations and will be presented later. However, we realise that, while we obtained a coherent description of the system at stationarity, the previous algorithm is not well suited to describe the evolution towards it. In fact, there is a problem in the dynamics of equations (3.11), in that they do not always respect the constraints for the maximum/minimum number of particles in the reservoirs. This means that we need to find new equations to describe the behaviour of the reservoirs if we want to explore the full dynamics of the system. What we need to do is to substitute equations (3.11) with two new sets of equations, one for each reservoir, that describe the time evolution of the probabilities for $R_{1,2}$ to be in a state with a specific number of particle r. We call these probabilities $p_{1,2}(r)$. In their equations, the information

on the constraints for the maximum/minimum number of particles in the reservoirs can be included. Also, with the new probabilistic viewpoint for the reservoirs, in equations (3.10) and in the injection/extraction currents inside this same new sets of equations, one has to substitute N_1,N_2 with their averages $\langle N_1\rangle$,$\langle N_2\rangle$ computed using $p_{1,2}(r)$. The form of the set of equations for the time evolution of $p_{1,2}(r)$ is a little bit cumbersome. We can write a more compact formulation by using the complementary cumulative distributions, defined as:

$$P_1(n) = \sum_{r=n}^{N_{TOT}} p_1(r) \tag{3.15}$$

$$P_2(n) = \sum_{r=n}^{L} p_2(r) \tag{3.16}$$

These allow us to write, for $n = 1, \dots N_{TOT}$:

$$\begin{aligned} &\frac{dP_1(n)}{dt} = \frac{d}{dt}\sum_{r=n}^{N_{TOT}} p_1(r) = \\ &- p_1(n)\left(k_1 \cdot n \cdot (1 - p_2(L)) + \frac{n}{L}\alpha(1-\rho_1)\right) + p_1(n-1)k_2\langle N_2\rangle, \end{aligned} \tag{3.17}$$

and, for $n = 1, \dots L$:

$$\begin{aligned} &\frac{dP_2(n)}{dt} = \frac{d}{dt}\sum_{r=n}^{L} p_2(r) = \\ &- p_2(n)\cdot k_2 \cdot n \cdot (1 - p_1(N_{TOT})) + p_2(n-1)\left(k_1\langle N_1\rangle + \beta\rho_L\left(1 - \frac{n-1}{L}\right)\right) \end{aligned} \tag{3.18}$$

Notice that the $n = 0$ cases are trivial since $P_1(0) = P_2(0) = 1$ so their derivatives vanish. This new formulation allows us, in combination with equations (3.9)-(3.10), to use an algorithm equivalent to the one presented before to recover the same information on the steady state previously acquired and to also examine the full dynamics of the system.

3.3 Constraints analysis

We stated, in the previous section, that equations (3.11) have the problem that the constraints on the number of particles in the reservoirs are not respected during the transient to stationarity. However, these equations are pretty simple and we would like to use them, together with (3.9)-(3.10), to investigate the possible steady states of the system. This is possible because, as we said before, at stationarity, the aforementioned constraints can be respected. To justify this claim, we start by restating the equations:

$$\begin{cases} \frac{d\rho_i}{dt} = \rho_{i-1}(1-\rho_i) - \rho_i(1-\rho_{i+1}) & \text{with } i = 2, \dots L-1 \\ \frac{d\rho_1}{dt} = \alpha\frac{N_1}{L}(1-\rho_1) - \rho_1(1-\rho_2) \\ \frac{d\rho_L}{dt} = \rho_{L-1}(1-\rho_L) - \beta(1-\frac{N_2}{L})\rho_L \\ \frac{dN_1}{dt} = k_2 N_2 - k_1 N_1 - \alpha\frac{N_1}{L}(1-\rho_1) \\ \frac{dN_2}{dt} = k_1 N_1 - k_2 N_2 + \beta(1-\frac{N_2}{L})\rho_L \end{cases}$$

We omitted the temporal dependence of the variables for easier readability. Now we can impose the stationarity conditions: $\frac{d\rho_i}{dt} = 0, \forall i$ and $\frac{dN_{1,2}}{dt} = 0$. We then define the reservoir densities $\phi_{1,2} = \frac{N_{1,2}}{L}$ and use the scaling $k_{1,2} = \frac{\kappa_{1,2}}{L}$ to reshape the previous equations into:

$$\begin{cases} \rho_i = \frac{\rho_{i-1}}{1-\rho_{i+1}+\rho_{i-1}} = g(\rho_{i-1}, \rho_{i+1}) & \text{with } i = 2, \dots L-1 \\ \rho_1 = \frac{\alpha\phi_1}{1-\rho_2+\alpha\phi_1} = g_1(\rho_2, \phi_1) \\ \rho_L = \frac{\rho_{L-1}}{\beta(1-\phi_2)+\rho_{L-1}} = g_L(\rho_{L-1}, \phi_2) \\ \phi_1 = \frac{\kappa_2\phi_2}{\kappa_1+\alpha(1-\rho_1)} = w_1(\rho_1, \phi_2) \\ \phi_2 = \frac{\kappa_1\phi_1+\beta\rho_L}{\kappa_2+\beta\rho_L} = w_2(\rho_L, \phi_1) \end{cases} \tag{3.19}$$

We can thus see that, in mean field approximation, at stationarity, it is true that the steady state is a solution of a fixed-point equation, namely

$$(\rho_1, \rho_2 \dots \rho_L, \phi_1, \phi_2) = G(\rho_1, \rho_2 \dots \rho_L, \phi_1, \phi_2),$$

where G is just a compact way of restating the information on the fixed-point iterations (3.19). Therefore, in order to prove that such a solution satisfies the physical constraints, we need to be sure that the variables obtained through the transformation G satisfy the same constraints as the original variables. These constraints are:

$$\rho_i \in [0,1]; \qquad 0 \leq \phi_1 \leq \tfrac{\kappa_2}{\kappa_1}; \qquad 0 \leq \phi_2 \leq 1.$$

We note that the inequalities for ϕ_1, ϕ_2 clearly follow from the ones for N_1, N_2. We also remind that the parameters $\alpha, \beta, \kappa_1, \kappa_2$ are non negative.

- We start with ρ_i, with $i = 2 \dots L-1$ and see that:

  $$\rho_i = \frac{\rho_{i-1}}{1-\rho_{i+1}+\rho_{i-1}} \overset{(1)}{\leq} \frac{1}{2-\rho_{i+1}} \overset{(2)}{\leq} \frac{1}{2-1} = 1.$$

  Where in (1) we used the fact that $\rho_{i-1} \leq 1$ and in (2) that $\rho_{i+1} \leq 1$. Also,

  $$\rho_i = \frac{\rho_{i-1}}{1-\rho_{i+1}+\rho_{i-1}} \overset{(1)}{\geq} \frac{\rho_{i-1}}{1+\rho_{i-1}} \overset{(2)}{\geq} 0.$$

  In (1) we used $\rho_{i+1} \geq 0$ and in (2) $\rho_{i-1} \geq 0$. We can proceed to do a similar check on the other variables.

- For ρ_1:

$$\rho_1 = \frac{\alpha\phi_1}{1-\rho_2+\alpha\phi_1} \overset{(1)}{\leq} \frac{\alpha\phi_1}{1-1+\alpha\phi_1} = 1$$

Using $\rho_2 \leq 1$ in (1).

$$\rho_1 = \frac{\alpha\phi_1}{1-\rho_2+\alpha\phi_1} \overset{(1)}{\geq} \frac{\alpha\phi_1}{1+\alpha\phi_1} \overset{(2)}{\geq} 0$$

Using $\rho_2 \geq 0$ in (1) and $\phi_1 \geq 0$ in (2).

- For ρ_L:

$$\rho_L = \frac{\rho_{L-1}}{\beta(1-\phi_2)+\rho_{L-1}} \overset{(1)}{\leq} \frac{1}{\beta(1-\phi_2)+1} \overset{(2)}{\leq} 1$$

Using $\rho_{L-1} \leq 1$ in (1) and $\phi_2 \leq 1$ in (2).

$$\rho_L = \frac{\rho_{L-1}}{\beta(1-\phi_2)+\rho_{L-1}} \overset{(1)}{\geq} \frac{\rho_{L-1}}{\beta+\rho_{L-1}} \overset{(2)}{\geq} 0$$

Having used $\phi_2 \geq 0$ in (1) and $\rho_{L-1} \geq 0$ in (2).

- For ϕ_1:

$$\phi_1 = \frac{\kappa_2\phi_2}{\kappa_1+\alpha(1-\rho_1)} \overset{(1)}{\geq} \frac{\kappa_2\phi_2}{\kappa_1+\alpha} \overset{(2)}{\geq} 0$$

Where in (1) $\rho_1 \geq 0$ and in (2) $\phi_2 \geq 0$ were used.

$$\phi_1 = \frac{\kappa_2\phi_2}{\kappa_1+\alpha(1-\rho_1)} \overset{(1)}{\leq} \frac{\kappa_2\phi_2}{\kappa_1} \overset{(2)}{\leq} \frac{\kappa_2}{\kappa_1}$$

Using, respectively, $\rho_1 \leq 1$ and $\phi_2 \leq 1$ in (1) and (2).

- Lastly, for ϕ_2:

$$\phi_2 = \frac{\kappa_1\phi_1+\beta\rho_L}{\kappa_2+\beta\rho_L} \overset{(1)}{\geq} \frac{\beta\rho_L}{\kappa_2+\beta\rho_L} \overset{(2)}{\geq} 0$$

Where we used $\phi_1 \geq 0$ in (1) and $\rho_L \geq 0$ in (2).

$$\phi_2 = \frac{\kappa_1\phi_1+\beta\rho_L}{\kappa_2+\beta\rho_L} \overset{(1)}{\leq} \frac{\cancel{\kappa_1}\frac{\kappa_2}{\cancel{\kappa_1}}+\beta\rho_L}{\kappa_2+\beta\rho_L} = 1$$

The constraint $\phi_1 \leq \frac{\kappa_2}{\kappa_1}$ was used in (1).

This procedure has shown that, at steady state, equations (3.11), together with (3.9)-(3.10), allow the system to maintain stationary states for which the constraints on the number of particles in the reservoirs are satisfied. We can then use these equations to obtain some information on the allowed stationary states that satisfy

the constraints. In fact, we would like to analyse the steady state behaviour of the system given that the constraints are satisfied and for various values of the control parameters $(\alpha, \beta, \mu, k_1, k_2)$. Interestingly, it is actually these constraints on the number of particles in the reservoirs that can guide us in this analysis. We will explain here how to do it, for the Weak Coupling case. The results will be presented in the next chapter.

Let us define the average density inside the TASEP as $\overline{\rho} = \frac{N_T}{L}$. We can use this definition, together with the ones for the reservoir densities and that of the filling factor, to restate the equation for the conservation of the number of particles in the system, eq.(2.14), as

$$\mu = \phi_1 + \phi_2 + \overline{\rho}. \tag{3.20}$$

We can also rewrite equations (3.11) in terms of the reservoir densities as

$$\begin{aligned} \frac{d\phi_1}{dt} &= k_2\phi_2 - k_1\phi_1 - \frac{\alpha}{L}\phi_1(1-\rho_1) \\ \frac{d\phi_2}{dt} &= k_1\phi_1 - k_2\phi_2 + \frac{\beta}{L}(1-\phi_2)\rho_L \end{aligned} \tag{3.21}$$

At stationarity, inside the TASEP, it is true that all the density currents are equal: $J_i = J, \forall i = 0, \dots L$. This means that in (3.21) we can rewrite the injection/extraction terms as J. Also, obviously, we have $\frac{d\phi_1}{dt} = \frac{d\phi_2}{dt} = 0$. By combining this information with the scaling $k_{1,2} = \frac{\kappa_{1,2}}{L}$, one can write a balance equation for the currents at stationarity

$$J + \kappa_1\phi_1 - \kappa_2\phi_2 = 0. \tag{3.22}$$

Combining this equation with (3.20) we can obtain two equations for the reservoir densities

$$\begin{aligned} \phi_1 &= \frac{\kappa_2(\mu - \overline{\rho}) - J}{\kappa_1 + \kappa_2} \\ \phi_2 &= \frac{\kappa_1(\mu - \overline{\rho}) + J}{\kappa_1 + \kappa_2} \end{aligned} \tag{3.23}$$

Considering that between the two reservoirs there is a pure TASEP, we can parameterise the density current as $J = \rho(1-\rho)$, with $\rho \in [\ 0, \frac{1}{2}]$, the smallest between the two possible bulk densities $\rho^{\pm} = \frac{1 \pm \sqrt{1-4J}}{2}$ that are coherent with J. We can therefore write

$$\begin{aligned} \phi_1 &= \frac{\kappa_2(\mu - \overline{\rho}) - \rho(1-\rho)}{\kappa_1 + \kappa_2} = f_1(\rho, \overline{\rho}) \\ \phi_2 &= \frac{\kappa_1(\mu - \overline{\rho}) + \rho(1-\rho)}{\kappa_1 + \kappa_2} = f_2(\rho, \overline{\rho}) \end{aligned} \tag{3.24}$$

What we have just obtained is a description of the reservoir densities in terms of the average density in the TASEP $\overline{\rho}$, the bulk density ρ and three control parameters.

This description is important because we can use it to understand, depending on μ, κ_1, κ_2, what physical phases the TASEP can be in. In order to do so, let us first remind what phases are allowed in the TASEP, in terms of $\rho, \overline{\rho}$, and the effective injection/extraction parameters $(\alpha_{EFF}, \beta_{EFF})$:

- LOW DENSITY (LD). Bulk density $\rho < \frac{1}{2}$ controlled by injection, $\rho^- = \rho = \alpha_{EFF}$ and $\overline{\rho} = \rho$. Boundary layer localised at the extraction side.

- HIGH DENSITY (HD). Bulk density $1-\rho > \frac{1}{2}$ controlled by extraction, with $\rho^- = \rho = \beta_{EFF}$ and $\overline{\rho} = 1-\rho$. Boundary layer localised at the injection side.

- COEXISTENCE REGION (DW), which can also be called Domain Wall phase. Two bulk densities $\rho(< \frac{1}{2})$ and $1-\rho(> \frac{1}{2})$, controlled by injection and extraction, respectively. It is true that $\rho^- = \alpha_{EFF} = \beta_{EFF}$ and $\overline{\rho} = x_{DW}\rho + (1-x_{DW})(1-\rho)$, where x_{DW} is the position of the domain wall that separates the two bulk densities.

- MAX CURRENT (MC). Two boundary layers and unique bulk density $\rho = \overline{\rho} = \frac{1}{2}$.

In the convenient plane representation below, we can easily see a summary of what we just listed:

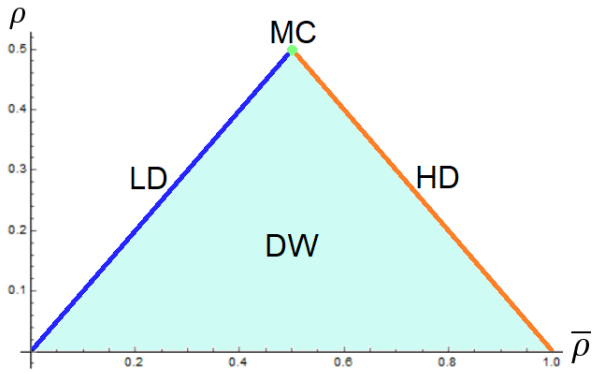

Figure 3.1: Allowed phases in the TASEP in $(\rho, \overline{\rho})$ plane. Phase tags are defined in the text.

We know that the reservoir densities have to abide by certain constraints. Namely:

$$0 \leq \phi_1 \leq \tfrac{\kappa_2}{\kappa_1}; \qquad 0 \leq \phi_2 \leq 1.$$

By substituting (3.24) into these constraints we get four inequalities that are used to create a surface in $(\rho, \overline{\rho})$ that can be superimposed on the plane representation of fig. 3.1 and can tell us the allowed phases that the TASEP can be in at stationarity, depending on the values of μ, κ_1, κ_2. We analysed these inequalities and produced a Wolfram Mathematica code that allows us to show a visual representation of the permitted phases for any combination of the control parameters. We will present these results in the next chapter.

If we briefly retrace the steps up to here, we can see that we started with some mean field equations to describe, in that approximation, the behaviour of the system TASEP+Reservoirs. Then, we showed that these equations can be used to analyse the stationary state of the system because they respect, at stationarity, the constraints on the number of particles in the reservoirs. After that, we used these constraints to guide us into understanding how to recover the phases that the TASEP can find itself in, at stationarity, depending on the values of μ, κ_1, κ_2. What is left to analyse is the role of the injection/extraction parameters α, β. It should be easily understandable that, while a chosen combination of μ, κ_1, κ_2 restricts the space of allowed steady states, the specific phase among the permitted ones that the system reaches is fixed by these last two parameters. Obviously, α and β are parameters that can be tuned a priori and independently from the others. However, we will show that the specific combination of μ, κ_1, κ_2 is responsible for the delimitation of different regions of behaviours, in the (α, β) plane. This makes sense since, as we know, the TASEP under investigation is characterised by some effective injection/extraction parameters

$$\begin{aligned} \alpha_{EFF} &= \alpha\phi_1 \\ \beta_{EFF} &= \beta(1-\phi_2) \end{aligned} \tag{3.25}$$

and these effective parameters are influenced by the reservoir densities that can be expressed as (3.24). We will now show how to use the previous information to distinguish the different regions of the (α, β) plane associated with each of the permitted phases.

Let us start with the coexistence or domain wall phase. I know that $\rho = \rho^- = \alpha_{EFF} = \beta_{EFF}$ and thus

$$\begin{aligned} \rho &= \alpha_{EFF} = \alpha_{DW}\phi_1 = \alpha_{DW} f_1(\rho, \overline{\rho}) \\ \rho &= \beta_{EFF} = \beta_{DW}(1-\phi_2) = \beta_{DW}(1 - f_2(\rho, \overline{\rho})) \end{aligned} \tag{3.26}$$

Hence,

$$\begin{aligned} \alpha_{DW}(\rho, \overline{\rho}) &= \frac{\rho}{f_1(\rho, \overline{\rho})} = \frac{\rho(\kappa_1+\kappa_2)}{\kappa_2(\mu-\overline{\rho}) - \rho(1-\rho)} \\ \beta_{DW}(\rho, \overline{\rho}) &= \frac{\rho}{1 - f_2(\rho, \overline{\rho})} = \frac{\rho(\kappa_1+\kappa_2)}{(\kappa_1+\kappa_2) - \kappa_1(\mu-\overline{\rho}) - \rho(1-\rho)} \end{aligned} \tag{3.27}$$

If we now set the condition $\overline{\rho} = \rho$, true for the low density phase, we obtain a parametric expression (with parameters $\rho \in [\ 0, \frac{1}{2}]\ , \mu, \kappa_1, \kappa_2$) for the boundary line between the low density and the domain wall phases in the (α, β) plane:

$$\alpha_{DW-LD}(\rho) = \alpha_{DW}(\rho, \rho) = \frac{\rho(\kappa_1 + \kappa_2)}{\kappa_2(\mu - \rho) - \rho(1 - \rho)}$$
$$\beta_{DW-LD}(\rho) = \beta_{DW}(\rho, \rho) = \frac{\rho(\kappa_1 + \kappa_2)}{(\kappa_1 + \kappa_2) - \kappa_1(\mu - \rho) - \rho(1 - \rho)}$$

In low density it is true that $\overline{\rho} = \rho$ and also that

$$\rho = \rho^- = \alpha_{EFF} = \alpha_{LD}\phi_1 = \alpha_{LD} f_1(\rho, \rho) \tag{3.28}$$

This means that $\alpha_{DW-LD} = \frac{\rho}{f_1(\rho,\rho)}$ is not only valid at the boundary between low density and domain wall but everywhere in the low density phase. Also, it means that this expression could be used to express the inverse relationship between α and the bulk density ($\overline{\rho} = \rho$). Hence,

$$\alpha_{LD}(\overline{\rho}) = \alpha_{DW-LD}(\overline{\rho}) = \frac{\overline{\rho}(\kappa_1 + \kappa_2)}{\kappa_2(\mu - \overline{\rho}) - \overline{\rho}(1 - \overline{\rho})} \tag{3.29}$$

We know that we have the possibility, given the last equation, to associate a specific value for α for any value of the bulk density $\overline{\rho} \in [\ 0, \frac{1}{2}]$. We also know that the transition between the low density phase and the max current one is smooth, in that there is no jump in the bulk density at the transition. Therefore, if we set $\overline{\rho} = \frac{1}{2}$ in $\alpha_{LD}(\overline{\rho})$ we can obtain the value of the injection parameter α at the transition between the low density and max current phases:

$$\alpha_{LD-MC} = \alpha_{LD}\left(\frac{1}{2}\right) = \frac{\frac{1}{2}(\kappa_1 + \kappa_2)}{\kappa_2(\mu - \frac{1}{2}) - \frac{1}{4}}. \tag{3.30}$$

Looking back at (3.27), if we now set the condition $\overline{\rho} = 1 - \rho$, true for the high density phase, we obtain a parametric expression for the boundary line between the high density and the domain wall phases:

$$\alpha_{DW-HD}(\rho) = \alpha_{DW}(\rho,1 - \rho) = \frac{\rho(\kappa_1 + \kappa_2)}{\kappa_2(\mu - 1 + \rho) - \rho(1 - \rho)}$$
$$\beta_{DW-HD}(\rho) = \beta_{DW}(\rho,1 - \rho) = \frac{\rho(\kappa_1 + \kappa_2)}{(\kappa_1 + \kappa_2) - \kappa_1(\mu - 1 + \rho) - \rho(1 - \rho)}$$

Similarly to the low density case, we can extend the DW-HD boundary result to the entire high density phase and, recalling now that $\overline{\rho} = 1 - \rho$, we can obtain

$$\beta_{HD}(\overline{\rho}) = \beta_{DW-HD}(1 - \overline{\rho}) = \frac{(1 - \overline{\rho})(\kappa_1 + \kappa_2)}{(\kappa_1 + \kappa_2) - \kappa_1(\mu - \overline{\rho}) - (1 - \overline{\rho})\overline{\rho}} \tag{3.31}$$

If we set $\overline{\rho} = \frac{1}{2}$ in $\beta_{HD}(\overline{\rho})$ we can obtain the value of the ejection parameter β at the transition between the high density and max current phases:

$$\beta_{HD-MC} = \beta_{HD}\left(\frac{1}{2}\right) = \frac{(\kappa_1 + \kappa_2)}{(3 - 2\mu)\kappa_1 + 2\kappa_2 - \frac{1}{2}} \tag{3.32}$$

We see that, as we claimed, we obtained expressions that define regions of the (α, β) plane for which, given a specific combination of μ, κ_1, κ_2, different steady state phases are obtained. We combined these expressions and wrote a Wolfram Mathematica code that can, for any combination of μ, κ_1, κ_2, produce a phase diagram in the (α, β) plane. These results are presented in the next chapter.

Chapter 4

Results

In this section, we are going to present and discuss the results obtained about the stationary state of the model in the Weak Coupling limit by means of the methods we have introduced previously. We remind that, with the term 'Weak Coupling' we refer to the situation in which diffusion between the reservoirs does not dominate the system dynamics and is in fact comparable with the hopping processes inside the TASEP. As explained in section 3.2, we ensure so by having the diffusion rates scale with the lattice size L like $k_{1,2} = \frac{\kappa_{1,2}}{L}$, with $\kappa_{1,2} \sim O(1)$.

4.1 Role of the constraints and admitted phases

In section 3.3, we have shown how we can obtain a set of equations for the reservoir densities (3.24), starting from some mean field considerations. We then explained how, given that the reservoir densities have to satisfy certain constraints, one can get a set of inequalities that can provide information on the allowed phases that the TASEP can be in at stationarity. These inequalities are:

1. $\phi_1 \geq 0 \longrightarrow \overline{\rho} \leq \mu - \frac{\rho(1-\rho)}{\kappa_2}$
2. $\phi_2 \geq 0 \longrightarrow \overline{\rho} \leq \mu + \frac{\rho(1-\rho)}{\kappa_1}$
3. $\phi_2 \leq 1 \longrightarrow \overline{\rho} \geq \mu - 1 - \frac{\kappa_2}{\kappa_1} + \frac{\rho(1-\rho)}{\kappa_1}$
4. $\phi_1 \leq \frac{\kappa_2}{\kappa_1} \longrightarrow \overline{\rho} \geq \mu - 1 - \frac{\kappa_2}{\kappa_1} - \frac{\rho(1-\rho)}{\kappa_2}$

Of these inequalities, only the first one and the third one are considered, given that the other two are less restricting. We then wrote a Wolfram Mathematica code that can delimit a region in $\rho, \overline{\rho}$, starting from the inequalities, and superimpose it on the plane representation of fig. 3.1. We show below an example of the output of this code.

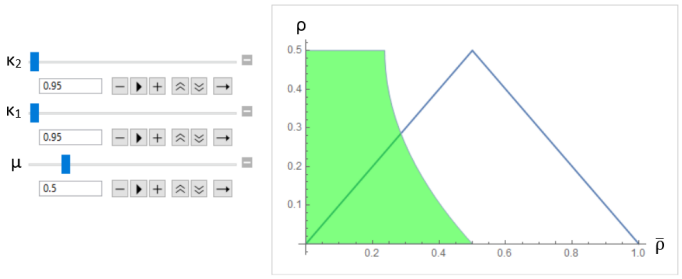

Figure 4.1: The coloured area denotes the allowed phase region at stationarity for the TASEP with parameters $\kappa_1 = \kappa_2 = 0.95, \mu = 0.5$.

As one can see, by fixing the values for the parameters κ_1, κ_2, μ, the resulting region created by the inequalities is laid over (and coloured in green) the diagram representing the possible phases of the TASEP. In this particular example, one infers that, for $\kappa_1 = \kappa_2 = 0.95, \mu = 0.5$, the allowed phases at stationarity are only the low density and the domain wall ones.

We also previously explained how we managed to obtain a series of expressions representing the separation lines among different phases in the (α, β) plane and wrote a Wolfram Mathematica code that can graphically depict a phase diagram. It is convenient to also show here an example of the output of this code, for the same parameters $\kappa_1 = \kappa_2 = 0.95, \mu = 0.5$.

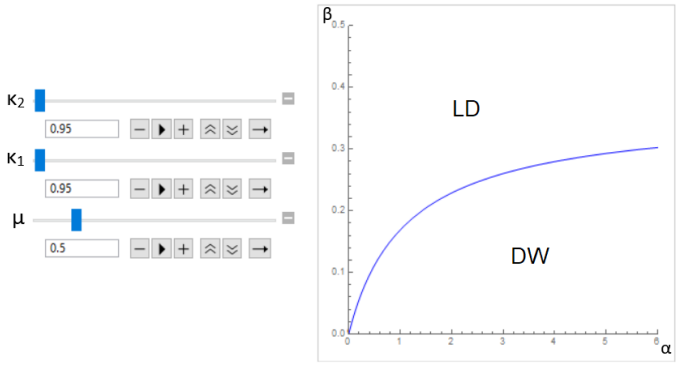

Figure 4.2: Phase diagram at stationarity in (α, β) for the TASEP with parameters $\kappa_1 = \kappa_2 = 0.95, \mu = 0.5$.

We could increase the limits of the previous diagram to show higher values of α, β but, as we would expect from the previous result, only the low density and domain wall phases would still appear.

We will use these codes, together with the Gillespie algorithm of section 3.1 and the numerical solution of the mean field equations of section 3.2 to investigate the rich and complex stationarity landscape of the system.

A first and important result we recover is that there is a necessary but not sufficient condition for the presence of a Maximal Current phase. The condition is that the diffusion rate κ_2 is higher than a critical value $\kappa_2^C = 0.25$. The reason we believe this condition arises is that this rate is the one that effectively participates in 'closing the circuit' formed by TASEP and reservoirs allowing the re-entry of particles (through R_1) at the beginning of the lattice and preventing a stop to the motion of the particles. One could expect that if this mechanism is not fast enough a situation of maximal current, i.e. maximal velocity of particles through the TASEP, cannot be sustained. We will show where one can extract this condition in a few paragraphs.

We can therefore now distinguish the cases for which Maximal Current can and cannot be present.

We find that when $\kappa_2 < 0.25$, the behaviour of the TASEP at stationarity is the following:

1. If $0 < \mu < 1$ the admitted phases are Low Density and Domain Wall;

2. If $1 < \mu < 1 + \frac{\kappa_2}{\kappa_1}$ the TASEP can be in every phase beside the Maximal Current one;

3. If $1 + \frac{\kappa_2}{\kappa_1} < \mu < 2 + \frac{\kappa_2}{\kappa_1} = \mu_{Max}$ the admitted phases are High Density and Domain Wall.

The separation values $(1,1 + \frac{\kappa_2}{\kappa_1})$ are found by examining the intersection of the surface created by the constraints on the diagram in fig. 3.1 for $\rho \sim 0$. Let us combine the Mathematica codes explained before to investigate, as an example, a situation with $\kappa_2 = \kappa_1 = 0.1 < 0.25$, for various values of μ ($\mu = 0.75, 1.3, 2.4$). We can show, in figure 4.3, for these values of these control parameters, what are the admitted phases and the phase diagrams for the TASEP. One can see that, for $\mu = 0.75 < 1$ (on the left side of fig. 4.3), the allowed phases are only the low density and the domain wall ones and the phase diagram is coherent with this notion. Increasing the value of μ, the LD-DW separation line rises up until the limit value $\mu = 1$, where its asymptotic behaviour changes from 'horizontal' to 'vertical' in the (α,β) plane. After $\mu = 1$, we enter the range in which the HD phase can appear. For $\mu = 1.3$ (in the middle of fig. 4.3) we have a coexistence of the three phases, as seen both on the phase diagram in $(\overline{\rho}, \rho)$ and (α, β). For higher values of μ the LD-DW separation line flattens on the β axis and the HD-DW boundary line rises. This happens up to the limit value $\mu = 2$, where the asymptotic behaviour of the HD-DW separation line changes from 'horizontal' to 'vertical' in the (α,β) plane and after which the Low Density phase disappears. For $\mu = 2.4 > 2$ (on the right side of fig. 4.3) the allowed phases are only the High Density and the Domain Wall ones. While μ increases up until μ_{Max} the HD-DW separation line flattens on the β axis.

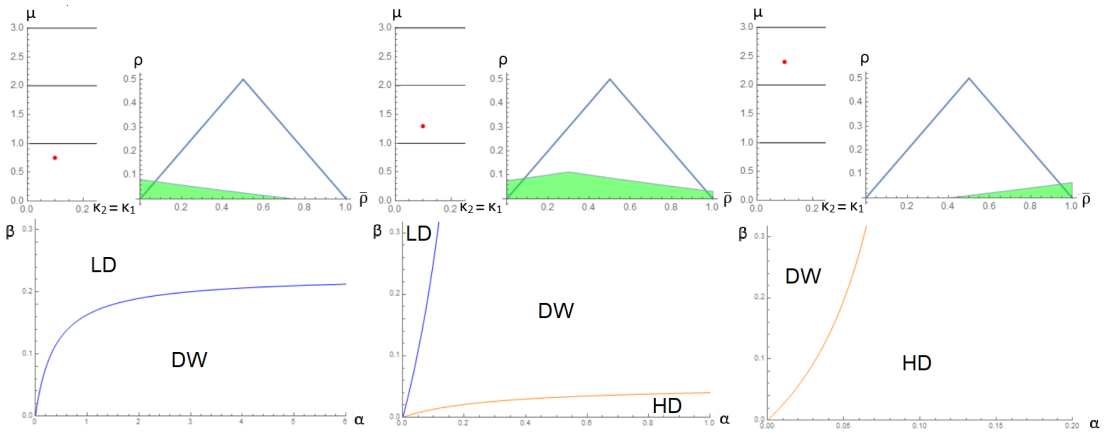

Figure 4.3: Phase diagrams at stationarity with $\kappa_2 = \kappa_1 = 0.1$ for various values of μ

Despite having considered, in the previous example, a case for which we had $\kappa_1 = \kappa_2$, the stationarity behaviour with μ does not qualitatively change (but there are quantitative differences, for example the limit value $1 + \frac{\kappa_2}{\kappa_1}$) when the diffusion rates are different (as long as $\kappa_2 < 0.25$).

Let us now look at the more complicated situation of $\kappa_2 > 0.25$, i.e. when a Maximal Current phase is possible:

1. If $0 < \mu < \frac{1}{2} + \frac{1}{4\kappa_2}$ the Low Density and Domain wall phases are present in the phase diagram. The High Density phase is admitted only if $\frac{1}{2} + \frac{1}{4\kappa_2} > 1$ for values of μ between these two limits;

2. If $\frac{1}{2} + \frac{1}{4\kappa_2} < \mu < \frac{3}{2} + \frac{\kappa_2}{\kappa_1} - \frac{1}{4\kappa_1}$, all phases are admitted;

3. If $\frac{3}{2} + \frac{\kappa_2}{\kappa_1} - \frac{1}{4\kappa_1} < \mu < 2 + \frac{\kappa_2}{\kappa_1}$ the High Density and Domain wall phases are present in the phase diagram. The Low Density phase is present only if $\frac{3}{2} + \frac{\kappa_2}{\kappa_1} - \frac{1}{4\kappa_1} < 1 + \frac{\kappa_2}{\kappa_1}$ for values of μ between these two limits.

When the limit value $\mu = 1$ ($\mu = 1 + \frac{\kappa_2}{\kappa_1}$) lies inside the range of existence for the Maximal Current phase ($\frac{1}{2} + \frac{1}{4\kappa_2} < \mu < \frac{3}{2} + \frac{\kappa_2}{\kappa_1} - \frac{1}{4\kappa_1}$), its effect is that of a topological change, in the phase diagram, for the behaviour of the HD(LD)-DW separation line. More precisely, for that specific value of μ, the line starts (ceases) to pass through the origin of the axes in the (α, β) plane. We will make this comment clearer with some examples later. It is now a good time to show where the limits ($\frac{1}{2} + \frac{1}{4\kappa_2}; \frac{3}{2} + \frac{\kappa_2}{\kappa_1} - \frac{1}{4\kappa_1}$) come from and, by consequence, where we can see a justification for the existence of the critical value $\kappa_2 = \kappa_2^C = 0.25$. If we look back at equations (3.30)-(3.32), we see that these are the parametric equations (with parameters μ, κ_1, κ_2) representing the critical values for the injection/ejection

parameters α/β at the transition between Low/High density and Maximal Current. We know that, for the existence of a Maximal Current phase, these two values must both exist and be positive. The two inequalities that follow from these requirements give, when combined, the range $\frac{1}{2}+\frac{1}{4\kappa_2}<\mu<\frac{3}{2}+\frac{\kappa_2}{\kappa_1}-\frac{1}{4\kappa_1}$. The prescription that $\frac{1}{2}+\frac{1}{4\kappa_2}<\frac{3}{2}+\frac{\kappa_2}{\kappa_1}-\frac{1}{4\kappa_1}$, when solved, gives the condition $\kappa_2>0.25$ that we stated as our first result as a necessary condition for the presence of a Maximal Current.

As we mentioned before, the present landscape (with $\kappa_2>0.25$) is more complicated and there are various different situations one can encounter for different combinations of κ_1,κ_2. First and foremost, we can produce some phase diagrams in μ,κ_2 for some fixed values of the ratio $\frac{\kappa_2}{\kappa_1}$. We find this representation to be quite interesting in that it can, at a glance, contain all the information on the different phases allowed. It can also contain information for the $\kappa_2<0.25$ case. Moreover, we note that it would be very impractical to try to read a three-dimensional diagram in $\mu-\kappa_1-\kappa_2$ containing all this information together. So, while not optimal, fixing the ratio $\frac{\kappa_2}{\kappa_1}$ and considering diagrams in μ,κ_2 seems to be our best practical solution to try to grasp the complexity we are dealing with. We show in the figure below that there are quite a few differences between various scenarios for the ratio $\frac{\kappa_2}{\kappa_1}$, be it less than, equal to, or bigger than one.

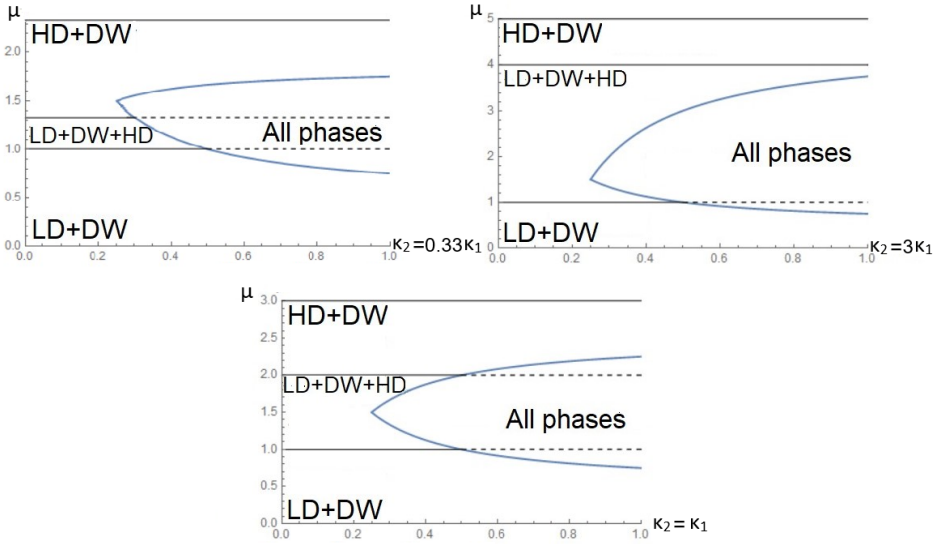

Figure 4.4: Phase diagrams in μ,κ_2 for $\frac{\kappa_2}{\kappa_1}=0.33,1,3$.

As one can see, there is a plethora of different situations that can arise. We can now take some combinations of parameters, one for each of the different ratios of fig. 4.4, and see what happens to the admitted phases and the phase diagram in (α,β) for increasing values of μ in an equivalent manner to what we did for $\kappa_2=\kappa_1=0.1$ before.

Let us start with $\kappa_1 = \kappa_2 = 0.95$, which corresponds to focus on a certain combination of parameters in the bottom diagram of fig. 4.4.

For $\mu = 0.5 < \frac{1}{2} + \frac{1}{4\kappa_2} \sim 0.76$ only the Low density and the Domain wall phases are admitted and therefore present in the phase diagram (see fig. 4.5a). Increasing μ, the domain wall region gets bigger, while there are still only these two phases, right up to the critical value $\mu \sim 0.76$, for which High Density and Maximal Current phases begin to appear. For $\mu = 0.9 < 1$ the four phases are present but the HD-DW separation line does not pass through the origin of the axes (see fig. 4.5b).

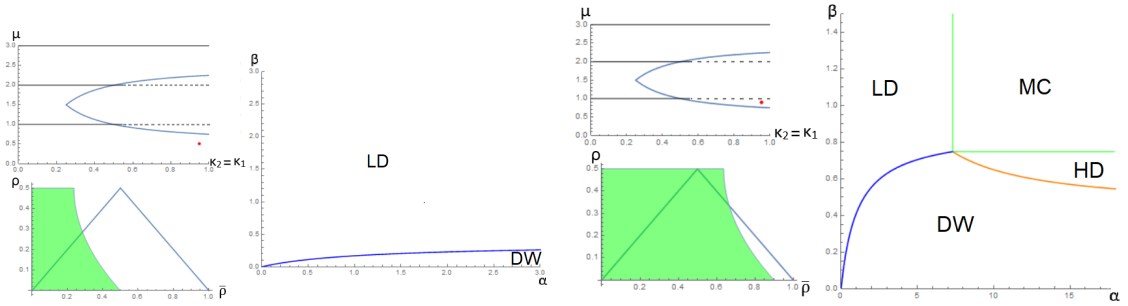

(a) $\mu = 0.5$ (b) $\mu = 0.9$

Figure 4.5: Phase diagrams for $\kappa_2 = \kappa_1 = 0.95$.

We can see in the figure below, that for $\mu = 1.5 > 1$, the four phases are present and the HD-DW separation line passes through the origin of the axes. This topological change seems to happen instantaneously when crossing the limit $\mu = 1$.

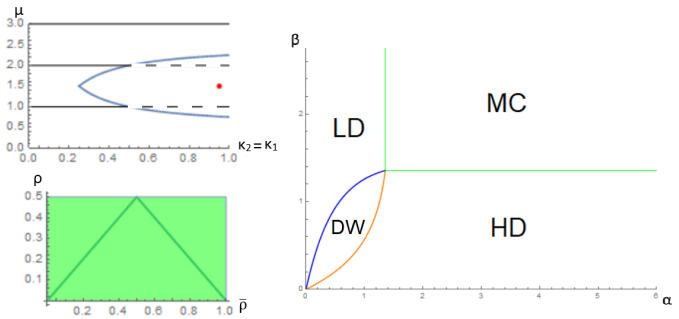

Figure 4.6: Phase diagram for $\kappa_2 = \kappa_1 = 0.95, \mu = 1.5$.

For $\mu = 2.1 > 1 + \frac{\kappa_2}{\kappa_1} = 2$ the four phases are present but the LD-DW separation line no longer passes through the origin of the axes (see fig. 4.7a). This has happened when crossing the limit line $\mu = 2$ in an opposite manner to the HD-DW separation line before. For $\mu = 2.5 > \frac{3}{2} + \frac{\kappa_2}{\kappa_1} - \frac{1}{4\kappa_1} \sim 2.24$ we exited the range that

allowed the presence of a Maximal Current phase and only the Domain Wall and the High density phases are present.

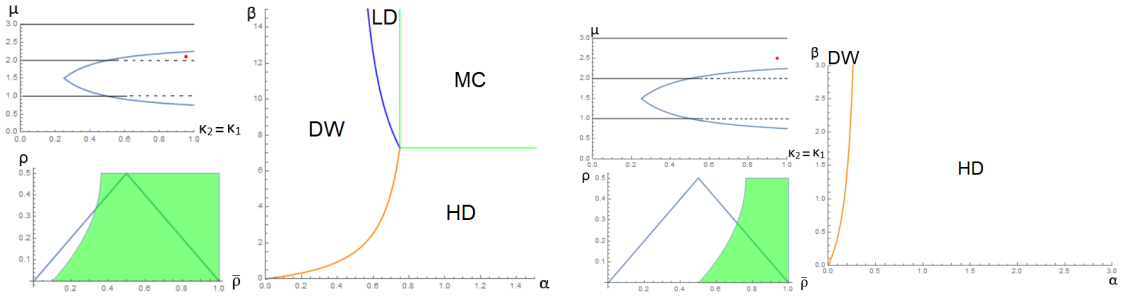

(a) $\mu = 2.1$ (b) $\mu = 2.5$

Figure 4.7: Phase diagrams for $\kappa_2 = \kappa_1 = 0.95$.

Before moving on we would like to mention the fact that when $\kappa_1 = \kappa_2$ the system has a particle-hole symmetry. This is manifest in the fact that the phase diagrams we presented are symmetrical with respect to $\mu = 1.5$ which is exactly half of $\mu_{Max} = 2 + \frac{\kappa_2}{\kappa_1} = 3$ in this case. What we mean by symmetrical is that, if one looks at the couples of values of μ equidistant to 1.5, like the shown cases of $\mu = 0.9$,2.1 or $\mu = 0.5$,2.5, it can be seen that, under the exchanges $\alpha \leftrightarrow \beta$, $\mu \leftrightarrow 3 - \mu$, the LD-MC phase boundary can be interchanged with the HD-MC one and LD-DW phase boundary can be exchanged with the HD-DW one and the resulting diagrams are identical. Also, the phase diagram in $\mu - \kappa_2$ is clearly symmetrical with respect to 1.5.

We can now move on to the case $\kappa_2 = 0.9, \kappa_1 = 0.3$, which corresponds to focus on a certain combination of parameters in the top right diagram of fig. 4.4.

For $\mu = 0.5 < \frac{1}{2} + \frac{1}{4\kappa_2} \sim 0.78$ only the Low Density and the Domain Wall phases are admitted and therefore present in the phase diagram (see fig. 4.8a). For $\mu = 0.85 < 1$ the four phases are present and the HD-DW separation line does not pass through the origin of the axes, as we would expect.

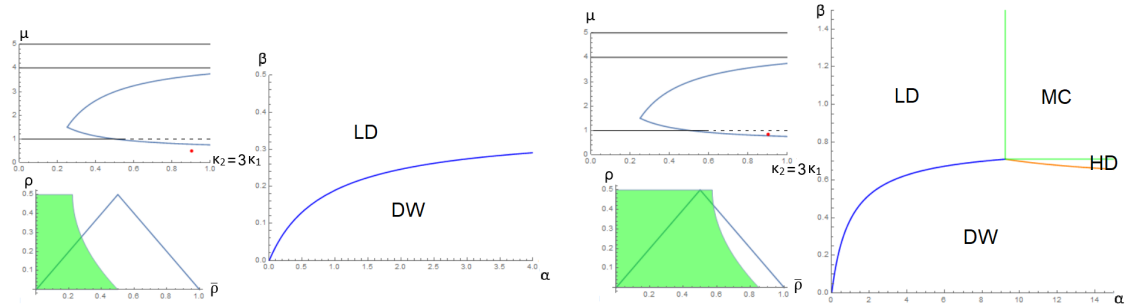

(a) $\mu = 0.5$ (b) $\mu = 0.85$

Figure 4.8: Phase diagrams for $\kappa_2 = 0.9, \kappa_1 = 0.3$.

When we increase μ up from 0.9 the HD region increases its size and the HD-DW phase boundary lowers itself closer to the α axis. Then at $\mu = 1$ there is the topological change and we can see for $\mu = 1.01$ the HD-DW phase boundary passes through the origin (see fig. 4.9a). If one keeps increasing μ the DW region gets smaller and we get the situation for $\mu = 2.4$ (see fig. 4.9b).

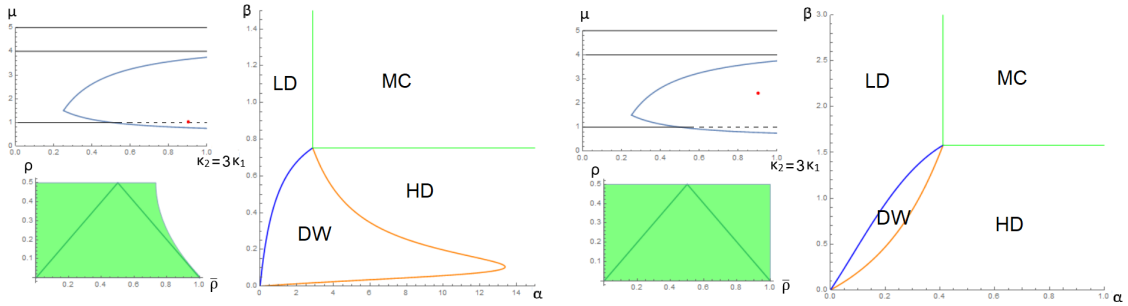

(a) $\mu = 1.01$ (b) $\mu = 2.4$

Figure 4.9: Phase diagrams for $\kappa_2 = 0.9, \kappa_1 = 0.3$.

Starting from $\mu = 2.4$ and increasing μ one can assist to a shift of the Maximal Current region for higher values of β up until $\mu = \frac{3}{2} + \frac{\kappa_2}{\kappa_1} - \frac{1}{4\kappa_1} \sim 3.7$, where the region disappears and we are left with just three phases as we can see on the left side of the figure below for $\mu = 3.8$. If we then cross the limit $1 + \frac{\kappa_2}{\kappa_1} = 4$ we are left only with HD and DW phases, which we can see on the right side of the figure below for $\mu = 4.1$.

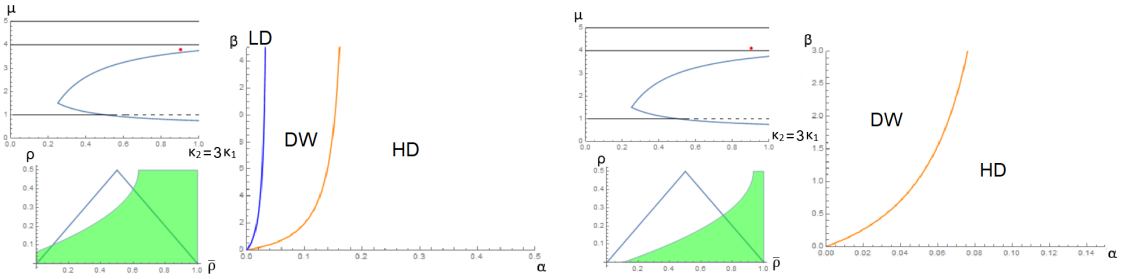

(a) $\mu = 3.8$ (b) $\mu = 4.1$

Figure 4.10: Phase diagrams for $\kappa_2 = 0.9, \kappa_1 = 0.3$.

Lastly, we consider the case $\kappa_2 = 0.33, \kappa_1 = 0.99$, which corresponds to focus on a certain combination of parameters in the top left diagram of fig. 4.4.

As one can see in the image below, for $\mu = 0.5 < 1$, only the Low Density and the Domain Wall phases are admitted and therefore present in the phase diagram. For $1 < \mu = 1.1 < \frac{1}{2} + \frac{1}{4\kappa_2} \sim 1.26$ the High Density phase is now allowed.

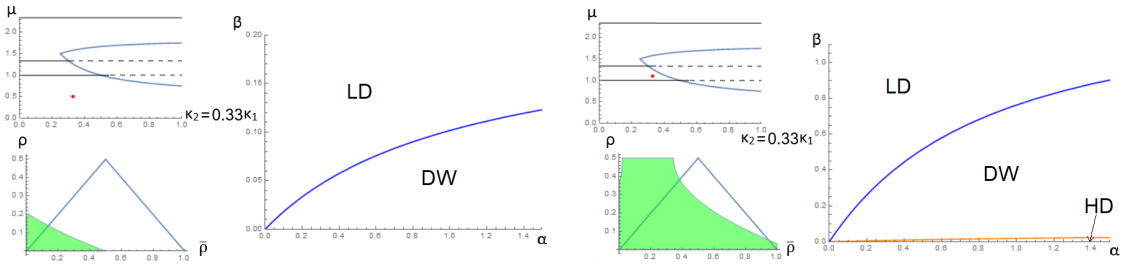

(a) $\mu = 0.5$ (b) $\mu = 1.1$

Figure 4.11: Phase diagrams for $\kappa_2 = 0.33, \kappa_1 = 0.99$.

When we cross the boundary line $\frac{1}{2} + \frac{1}{4\kappa_2} \sim 1.26$ we know we enter the range of values for which all the phases are allowed and that is shown in the next figure. We have two interesting features to notice in this diagram. First of all, we can look at the shape of the LD-DW boundary line and see that evidently something is happening. What we are seeing is simply the modification of this boundary line that, as we get closer to the limit value $\mu = 1 + \frac{\kappa_2}{\kappa_1} = 1.33$, changes its shape to then perform the topological jump we talked about before and stops passing through the origin. Secondly, we see that the HD-DW boundary line looks to be split into two branches and this looks unfamiliar, we will comment more about it later.

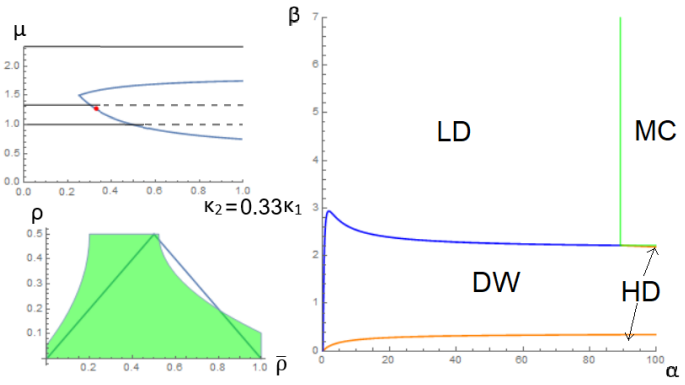

Figure 4.12: Phase diagram for $\kappa_2 = 0.33, \kappa_1 = 0.99, \mu = 1.28$.

When crossing the limit $\mu = 1 + \frac{\kappa_2}{\kappa_1} = 1.33$ but staying inside the region in which Maximal Current is allowed we have four phases and now the LD-DW boundary line no longer passes through the origin, as one can see from the left side of the next image. As for the HD-DW boundary line, we now have a more common situation of having only one continuous line. In the end, increasing μ, we enter the zone where only High Density and Domain Wall are allowed and that is what we see on the phase diagram.

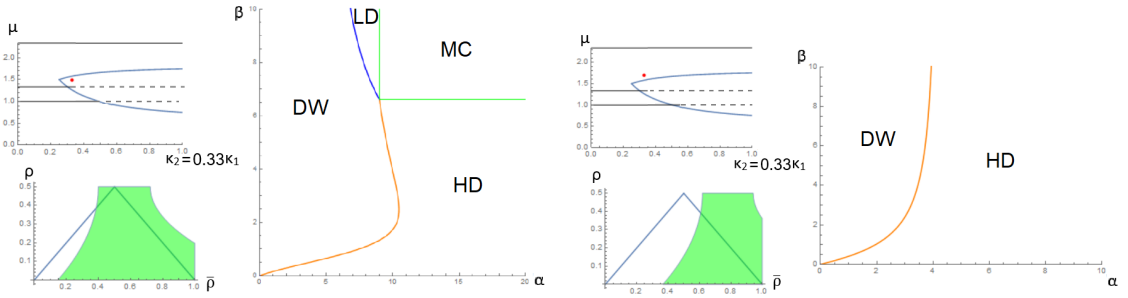

(a) $\mu = 1.43$ (b) $\mu = 1.7$

Figure 4.13: Phase diagrams for $\kappa_2 = 0.33, \kappa_1 = 0.99$.

To conclude this section, we would like to make a few comments. First of all, the investigation of this thesis has taken place keeping in mind the work [17], which we already mentioned quite a few times previously. It is sensible that we try to put the results we obtained into perspective and compare them with this work. When examining the situation for which $\kappa_1 = 0.01, \kappa_2 = 0.95$ (pag. 8 of the article), the authors stated that, for big values of μ, for example $\mu = 30$ and up to μ_{Max}, the only admitted phases (given their mean field calculations) are the High Density and Maximal Current ones. Their simulations seem to give four phases but, as we will explain later, we do not seem to agree quantitatively with any of their simulations. It seems from our analysis instead, that this situation is akin to the previous case where we had $\kappa_2 > \kappa_1$ (top right side of fig. 4.4). We find that for $\mu = 30$ and increasing μ until the limit $\frac{3}{2} + \frac{\kappa_2}{\kappa_1} - \frac{1}{4\kappa_1} (= 71.5)$ we have four phases. When $\frac{3}{2} + \frac{\kappa_2}{\kappa_1} - \frac{1}{4\kappa_1} < \mu < 1 + \frac{\kappa_2}{\kappa_1}$ we do not have the maximal current phase. In the end, for $1 + \frac{\kappa_2}{\kappa_1} < \mu < 2 + \frac{\kappa_2}{\kappa_1}$ (so $96 < \mu < 97$) only the High Density and Domain Wall phases are present. We can show here the phase diagram we obtain for $\kappa_1 = 0.1, \kappa_2 = 0.95, \mu = 30$.

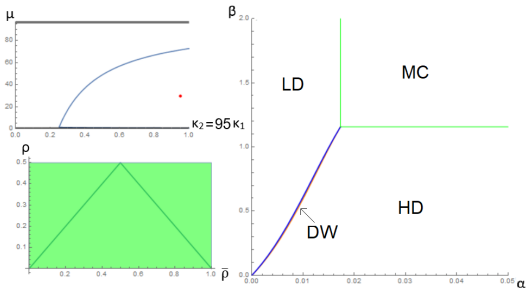

Figure 4.14: Phase diagram for $\kappa_2 = 0.95, \kappa_1 = 0.01, \mu = 30$.

Another comment we want to make regards a topologically interesting case for the phase diagram that we already encountered in fig. 4.12. If we consider the

situation $\kappa_2 = 0.7, \kappa_1 = 0.3, \mu = 1.01$ in the figure below we notice something interesting.

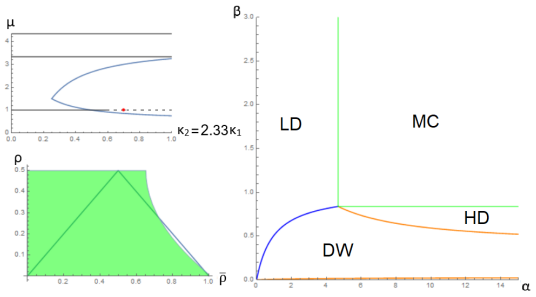

Figure 4.15: Phase diagram for $\kappa_2 = 0.7, \kappa_1 = 0.3, \mu = 1.01$.

We can see, looking in the $(\overline{\rho}, \rho)$ plane, that there is a zone of the High Density phase of non-admitted values contained between two zones of admitted values. The effect in the (α, β) plane is that of having two different branches for the parametric line that separates the Domain Wall and two detached zones of High density phases. Slightly increasing μ we can come to a more familiar situation for which all the high density values are admitted and the separation line is constituted by a unique branch that passes through the origin. Also, for values of $\frac{1}{2} + \frac{1}{4\kappa_2} < \mu < 1$ we had a single branch that did not pass through the origin. In the majority of the previous examples we did not have a similar situation, we instantaneously passed from a configuration for which the HD-DW separation line did not pass through the origin to one for which it did. This situation happens for other combinations of parameters, like the case presented before with $\kappa_1 = 0.99$, $\kappa_2 = 0.33$, $\mu = 1.28$. However, while we wanted to mention this specific phenomenon, we do not yet have a clear understanding of when and why it could arise or if there can be an equivalent situation with the LD-DW boundary phase. We will mention it more explicitly in the conclusions but it seems clear to us that the richness and complexity of the stationarity landscape for the system under investigation require more study that could bring enrichment to the phase diagrams obtained in this thesis.

We now move on to the next section where we will show how the Gillespie algorithm and the numerical solution of the mean field equations will show agreement with the phase diagrams presented here.

4.2 Stationary States: Mean Field and Kinetic Monte Carlo

Having obtained numerous phase diagrams while exploring the role of the control parameters on the possible existence of different stationary states, it is now paramount to show how qualitatively and quantitatively the mean field and kinetic Monte Carlo results that we produced agree with those predictions. Of course, we expect the mean field results to perfectly agree with the previous ones, obtained in the same approximation. The following results are obtained, if not stated otherwise, with a lattice size $L = 100$. Also, we let the system evolve for at least $T = 10^7$ transitions when running our Gillespie algorithm. Finally, we remind that the parameter ζ, defined in section 3.2 and used in our mean field code to indicate when stationarity is sufficiently close, stops the algorithm when its value stays below $1 \cdot 10^{-12}$. It must be noted that it is obviously not computationally feasible to re-obtain the previous phase diagrams point by point and with precise transition lines just by running some codes that can provide information on the specific stationary states given a defined set of control parameters. Therefore, what we will do in the following is to limit ourselves to overlay a specific grid of points on certain phase diagrams from the previous section and use this rough discretisation to run the codes on a finite number of points that, albeit small, could support our claims on the different regions and the boundaries between them in the (α, β) diagrams. Also, we will show what happens to the particle density profiles in the various cases. In principle, this analysis could be done for any combination of the control parameters. We performed it on all the cases of section 4.1, but, to avoid redundancy, we chose just a few examples to be shown here. Also, so as not to be repetitive, we decided to use different examples to showcase different facets of our investigation.

Let us start with the case for which a Maximal Current phase cannot be present, i.e. when $\kappa_2 < 0.25$, and consider $\kappa_2 = \kappa_1 = 0.1$, as we did in figure 4.3.

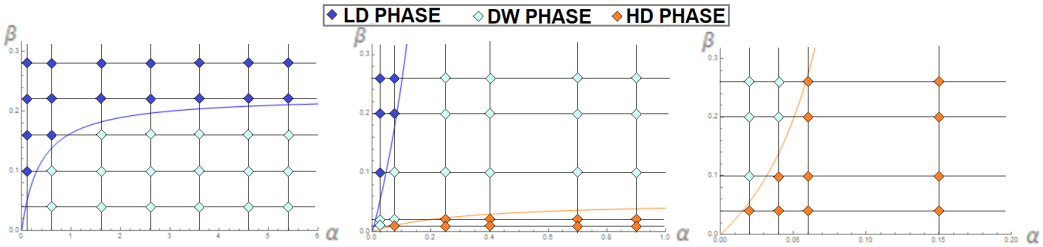

Figure 4.16: Phase diagrams at stationarity with $\kappa_2 = \kappa_1 = 0.1$ for $\mu = 0.75, 1.3, 2.4$. The coloured solid lines are the boundaries obtained in the previous section while the discrete points represent the phases obtained with MF and KMC codes.

As we can see, we can approximately reconstruct entire phase diagrams by discretising the phase space and using our codes to infer what steady state is reached for certain combinations of the control variables. Obviously, we are in control of both the number of grid points considered and their (in principle uneven) spacing and we can tune these parameters to our advantage to minimise the computations required while still checking the predictions of the theoretical results. A priori, one should be careful and use different markers for the stationary states obtained using our numerical mean field calculations and the Monte Carlo simulations. However, and we will talk more about it later, we merge the notation since we never found disagreement (in terms of stationary phase predicted by the two codes) between the results of the two methods. Of course, we find quantitative differences in the density profiles, though limited to the boundary layers and in the vicinity of the shock profile (Domain Wall phase). We use figure 4.17 to show the output obtained, both in mean field and through simulations, for the particle density for three different points, one for each possible phase, in the previous diagrams.

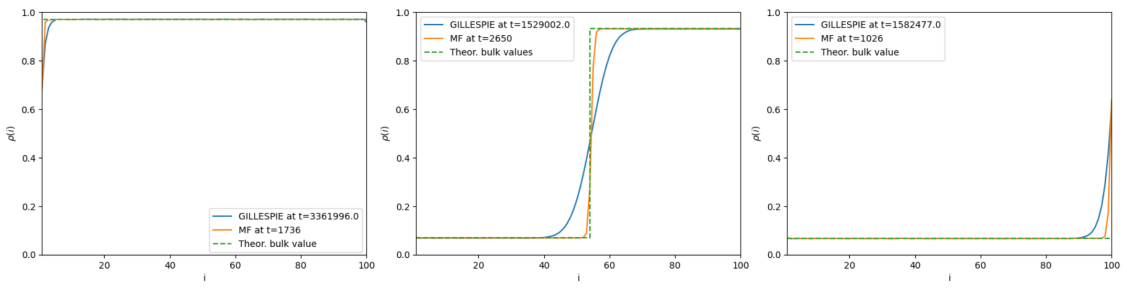

Figure 4.17: MF and KMC density profiles compared with (MF) theoretical bulk density for $\kappa_2 = \kappa_1 = 0.1$. Left panel: $\mu = 0.75, \alpha = 2.6, \beta = 0.28$. Center panel: $\mu = 1.3, \alpha = 0.7, \beta = 0.26$. Right panel: $\mu = 2.4, \alpha = 0.15, \beta = 0.2$.

As expected, no matter the particular phase or diagram considered, the different methods yield the same results in terms of the specific stationary state that they predict. In each panel in figure 4.17, we notice that there are three lines. Two correspond to the density profile obtained with the MC and MF codes, while the third is the theoretical bulk value that mean field predicts for those specific combinations of control parameters. We barely touched upon it, but in section 3.3 we mentioned that equation (3.29) could be inverted to express the relationship between α_{LD} and the bulk density. By doing so one can then find the bulk density $\overline{\rho}$ as a function of $\alpha_{LD}, \mu, \kappa_1, \kappa_2$. The same can be done for the High Density and then Domain Wall phase, while the bulk density predicted in the MC case is trivially $\overline{\rho}$=0.5. We can clearly see, in these examples, that there are quantitative differences between the density profiles obtained with the two methods around the shock for the DW phase and in general near the boundaries of the TASEP, as one could expect when

comparing simulations and mean field approximations. We could decide to investigate whether the bulk density shows a convergence to the theoretical value when increasing the size of the system, both for the MF and the KMC codes. This is certainly the way to proceed. In the spirit of not repeating ourselves and using different examples to show the different techniques we used, we will do this procedure for the next example. Finally, for this case, we should add that while here we plotted just a few particle densities and referred to figure 4.16 to show the various phase transitions in (α, β), there are other ways to do so. For example, we could produce a single graph containing various particle densities for different values of α and β, possibly along the line of a 'path' in the phase diagram, that could show the changes between phases. We will do so later in the section, for another phase diagram.

Moving on, let us analyze a case for $\kappa_2 > 0.25$. We consider here $\kappa_2 = \kappa_1 = 0.95$, with $\mu = 1.5$, so that we can compare our results with those in [17].

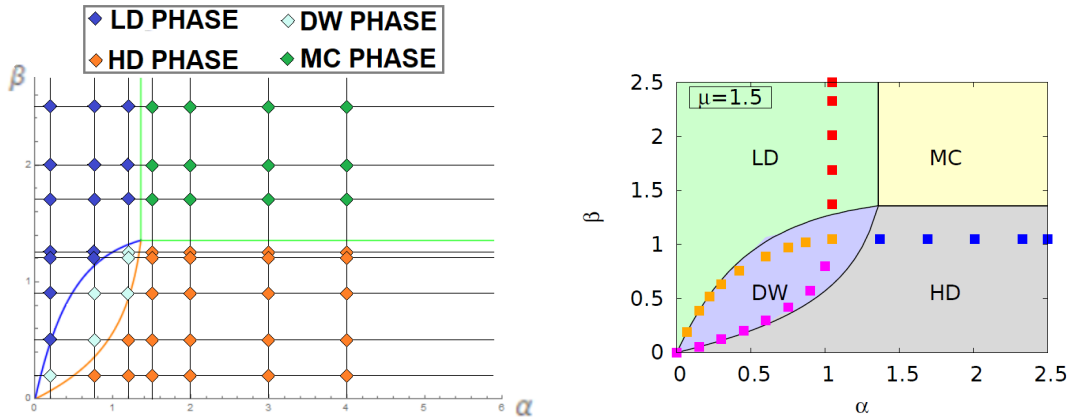

(a) Picture produced by the author. The coloured solid lines are the boundaries obtained theoretically while the discrete points represent the phases obtained with MF and KMC codes.

(b) Picture taken from [17]. The coloured regions separated by solid black lines are obtained in mean field. The discrete coloured points represent the phase boundaries obtained with Monte Carlo simulations.

Figure 4.18: Phase diagrams with $\kappa_2 = \kappa_1 = 0.95$ and $\mu = 1.5$.

First, we can again notice the excellent agreement between the theoretical predictions on the different steady states, with their respective regions on the phase diagram 4.18a, and the numerical and computational evaluations. This seems to be a remarkable improvement on the results obtained in [17]. The authors, as shown in 4.18b, state that their mean field predictions and Monte Carlo simulations do not quantitatively agree on the boundaries between the different phases. In some other examples, they find that the two sets of results also disagree on the number of phases present in the same diagram. They attribute this, and we quote (page

17), to 'stronger fluctuations in the weak coupling limit of the model'. However, we do not agree with the evidence they present to support this claim since, while we are only showing one example here, we reproduced all the phase diagrams present in the article and always seemed to find an optimal match between mean field approximations and the simulations. We can also use the example we just presented to show how the bulk density can converge to the theoretical value expected when one increases the size of the system, thus reducing the influence of finite-size effects. This should be self-evident through figure 4.19, where one can see, on the left side, the particle density as a function of the scaled position variable i/L obtained, for various L, using the code to numerically solve the mean field equations. On the right, instead, the same quantities are produced through Monte Carlo simulations. We chose two combinations of parameters close enough to the transition lines in figure 4.18a, bearing in mind the increasing difficulties of reaching numerical convergence the closer one gets to the transitions. Noticeably, the top row case in figure 4.19 corresponds to a set of parameters for which the authors in [17] find disagreement between their MF and MC results, at odds with what we can see.

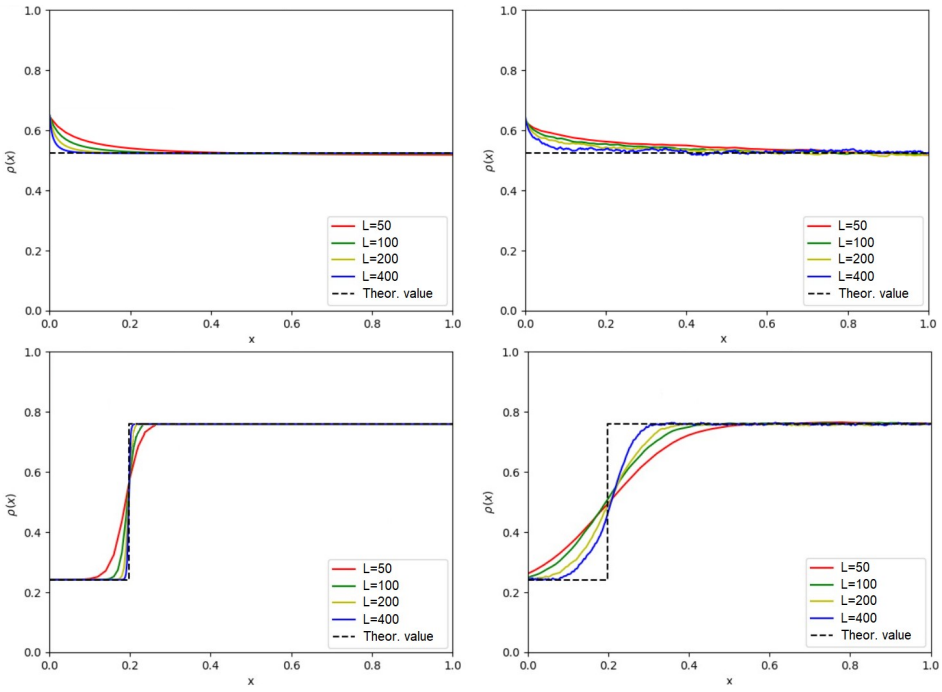

Figure 4.19: Particle densities obtained by mean field (left side) and Gillespie (right side) algorithms for different TASEP sizes as a function of the scaled position variable i/L. Top row: HD phase, $\alpha = 2, \beta = 1.25$. Bottom row: DW phase, $\alpha = 0.74, \beta = 0.5$. The black dashed lines denote the infinite-size (hydrodynamic) limit, obtained by the mean-field theory.

Lastly, let us consider the combination of parameters $\kappa_2 = 0.95, \kappa_1 = 0.01$, and $\mu = 2$, which is also one of the many cases for which the numerical and computational results in [17] disagree.

We have sketched, in the phase diagram of figure 4.20, some paths in the (α, β) plane along which we have highlighted a few specific points, in such a way as to sample the parameter space in every region while also looking closely at the boundaries between them. In figure 4.21, we show the behaviour of the particle densities along these paths, both in mean field and through simulations. While, of course, the results just presented are not nearly enough to reconstruct a phase diagram, we again emphasize here both the coherence of the two methods and, most importantly, the power they hold in how they can be, and have been, used to support the correctness of the phase diagrams obtained theoretically via the means previously described in sections 3.3-4.1.

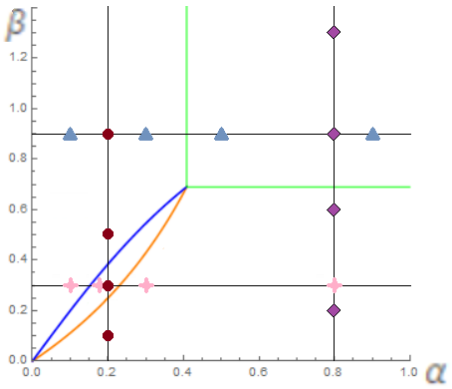

Figure 4.20: Phase diagram for $\kappa_2 = 0.95, \kappa_1 = 0.01, \mu = 2$

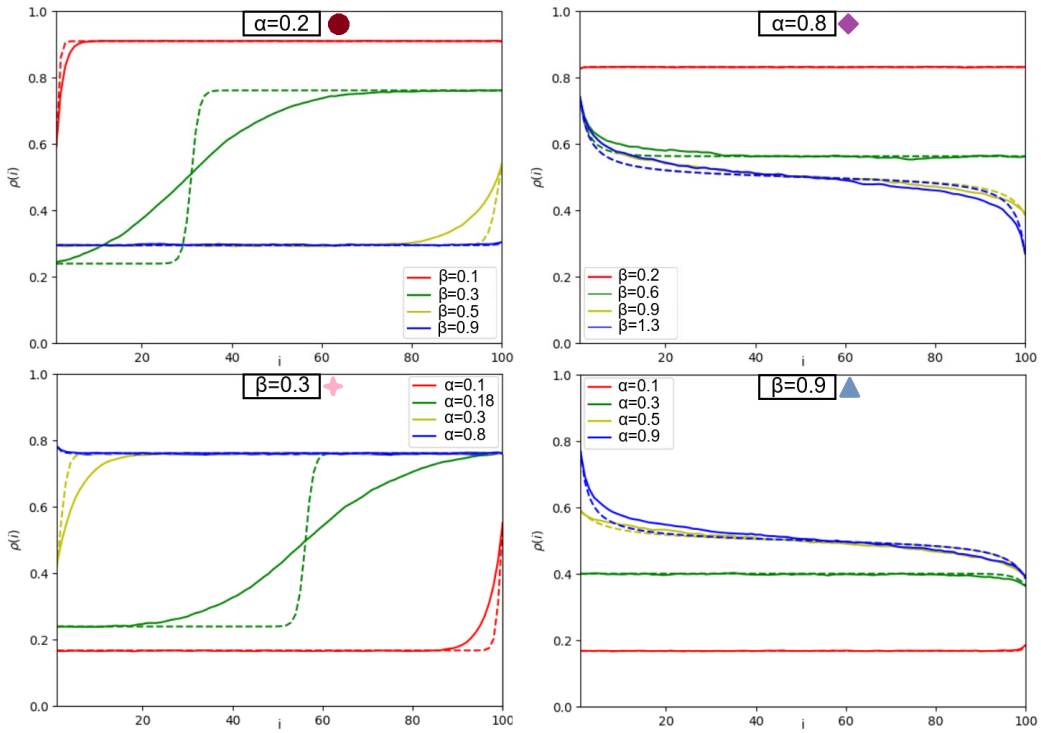

Figure 4.21: Particle densities obtained with mean field (dashed lines) and Gillespie (solid lines) algorithms for different combinations of the control parameters.

4.3 Full dynamics in Mean Field

Having discussed at length the stationary states of the system and after having shown agreement between the mean field approach and the simulations, we can now focus on the full dynamics. To do so we use an algorithm equivalent to that presented in section 3.2, based on equations (3.9)-(3.17)-(3.18). We choose as initial condition specific values for the variables that correspond to having an empty lattice and all the particles in the first reservoir at time $t = 0$, so $\rho_i = 0 \; \forall i$, $p_1(N_{TOT}) = 1$, $p_2(0) = 1$. This can be done without loss of generality, given that the stationary state is unique. We choose, for the examples below, $L = 50$ in order to not completely hide any finite-size effects. Also, in the figures of this section, the highest time shown is the one that corresponds to reaching stationarity. Let us consider the phase diagram of fig. 4.6, obtained for $\kappa_2 = \kappa_1 = 0.95, \mu = 1.5$. We will show the full dynamics to any possible stationary phase, through different combinations of α and β. In principle, we could do the same for every phase diagram of section 4.1, but we would find qualitatively similar behaviours.

We start with $\alpha = 0.5, \beta = 2$. For this choice of parameters, the stationary state is in the Low Density phase. In figure 4.22 we show the density profile at various times up to stationarity.

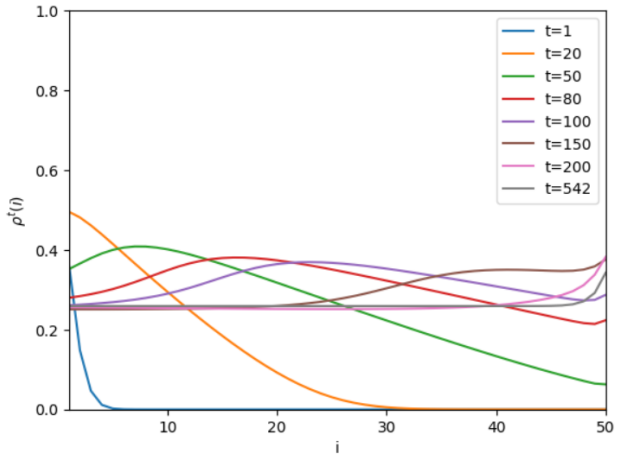

Figure 4.22: Density profile, at various times, for $\alpha = 0.5$, $\beta = 2$ (Low Density phase).

We can see, for short times, that the particles start entering the lattice from R_1 and the density profiles have a clear bump on the left side and then decay to zero since the particles have not had the time to travel a larger distance inside the lattice. After the time elapsed is of the order of the system size, the first particles entered will hit the right boundary of the lattice and start to move to R_2. We must now remind that the governing parameters of the TASEP in our system are the

effective injection/extraction ones $\alpha_{EFF}, \beta_{EFF}$, defined in equations (2.15). Those parameters depend on the reservoir densities $\phi_{1,2} = \frac{N_{1,2}}{L}$, which vary over time. Therefore the dynamics is not as straightforward as that of a TASEP connected to infinite non-interacting reservoirs. In that simpler system the filling of the lattice, in a Low Density case, corresponds to having a region of constant density α that gets larger with time up to the right boundary, where then a shock profile forms. Here, instead, given the initial condition, we have a surplus of particles near the entrance of the lattice that produces a bump in the density profile in that zone. With time, the number of particles in the first reservoir decreases and that of the second reservoir increases and this makes it so the injection and ejection processes are slowed down. The bump caused by the initial surplus of particles flattens and the system settles into the stationary situation for which the reservoir densities and therefore the effective injection/extraction parameters remain constant with time. On the right side, a shock profile is formed and connects the bulk density to the boundary value $1 - \beta_{EFF}$. The shock does not move since its velocity is positive.

We have seen how the profile density behaves during the complete dynamics to stationarity in this Low Density case. We can show what happens to the reservoir densities during this time. In figure 4.23 we can see two examples. On the left, we have the situation corresponding to the previous example of figure 4.22. Right until the time is of the order of the system size we can say that the diffusion mechanism dominates the filling of R_2, then the lattice ejection starts to contribute more until the system reaches stationarity.

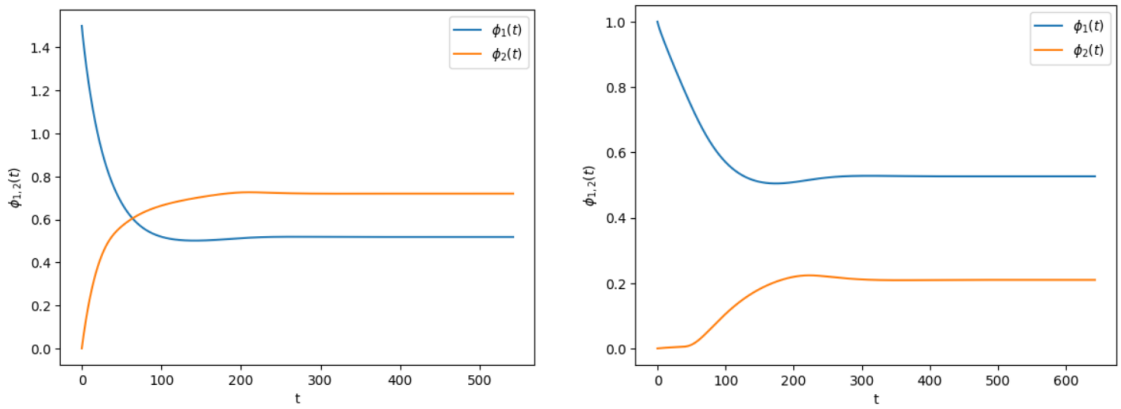

Figure 4.23: Time evolution of the reservoir densities for different values of the control parameters.

On the right, we have the dynamics of the reservoir densities for $\kappa_2 = 0.95, \kappa_1 = 0.01, \mu = 1$, $\alpha = 0.5$, $\beta = 0.9$, which also corresponds to a Low Density state. As we can see, for short times, below the order of the system size, the filling of R_2 is extremely slow, since the particles have not had enough time to reach the right side of the TASEP and the diffusion from R_1 plays a negligible role, given the tiny value

of κ_1. Also, we notice that the decrease of ϕ_1 is slower in time, for short times, compared to the previous case, because of the value of κ_1. Despite the chosen initial condition and resulting steady state, those represented in the picture are qualitatively the only two situations which can occur, i.e. either at stationarity the more filled reservoir is the same as the one at $t = 0$ or the opposite. We must stress that, theoretically, through mean field analysis and also thanks to the simulations, we already knew the values for the density profiles and the reservoir densities at stationarity. However, since we have here the full dynamics for these quantities, there is more work that can be done in the future concerning the time and the way in which stationarity is reached. We will mention this again in the conclusions.

Let us now return to the representation of the full dynamics of the various possible stationary states. We set $\alpha = 3$, $\beta = 2$, for which we expect a Maximal Current phase. We can see in figure 4.24a the evolution towards it and that no shock is present.

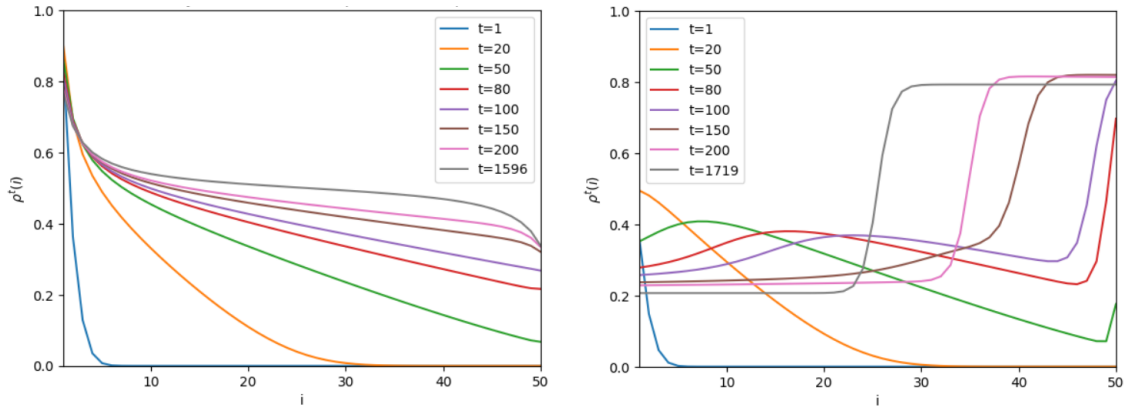

(a) MC phase, for $\alpha = 3$, $\beta = 2$.

(b) DW phase, for $\alpha = 0.5$, $\beta = 0.5$.

Figure 4.24: Density profile, at various times, for two different phases.

Conversely, if we take $\alpha = 0.5$, $\beta = 0.5$, the resulting stationary state, which we called Domain Wall phase, can be viewed as a coexistence of a Low Density and a High Density phase. There is a localised shock, clearly visible in figure 4.24b, whose position depends on the control parameters α, β, κ_1, κ_2, μ.

In the end, let us look at the evolution towards a High Density phase. We consider $\alpha = 1.5$, $\beta = 0.5$. We see in figure 4.25 that a shock is formed at the extraction side and then moves to the left until it reaches the left boundary where it settles, connecting the bulk density to the boundary value α_{EFF}. One could argue that the shock velocity, similarly to what happens in the infinite non-interacting reservoirs case, depends on the injection/extraction parameters as $|v_s| = \beta_{EFF} - \alpha_{EFF}$ and thus now depends on time. However, further analysis must be done to effectively prove this statement and we reserve it for future works.

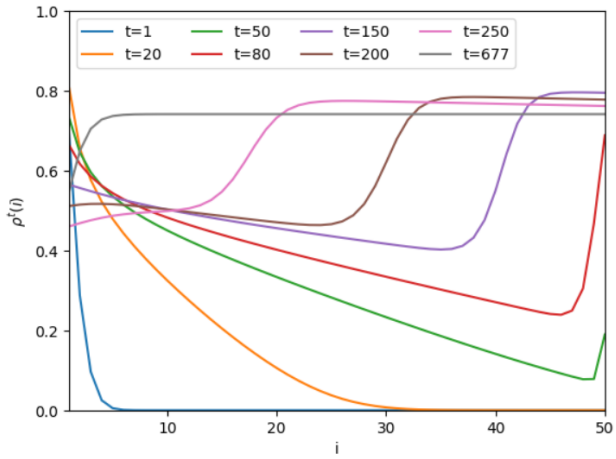

Figure 4.25: Density profile, at various times, $\alpha = 1.5$, $\beta = 0.5$ (High Density phase).

We might also add that when we increase the value of α we come to a situation for which the full shock dynamics seem to be practically independent of this parameter, as shown in figure 4.26. This reminds us of the situation, occurring in the simpler case of the TASEP with OBC (section 2.2), for which one can define some lines in the phase diagram that represent so-called 'dynamical transitions', after which this same kind of behaviour is present. These transitions do not correspond to any stationary state change, but separate regions within the same phase for which the relaxation towards stationarity has different characteristics. Nevertheless, this is all speculation at this stage and requires more investigation.

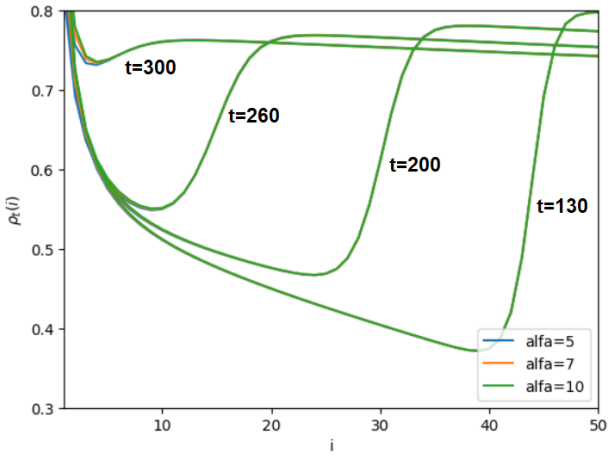

Figure 4.26: Full density profiles at different times for various values of α

Before moving on to the conclusions, we would like to expand on a comment we made in section 3.2. We explained that the first dynamics we proposed, and the associated code to numerically solve the corresponding equations, resulted in having a good representation of the system at stationarity, while not being appropriate to describe the evolution towards it. In fact, we noticed a problem in the dynamics in that the constraints for the number of particles in the reservoirs were not always respected. This prompted us to revise the equations and write a second code. We did, and the results presented in this section were derived using said algorithm. It would be useful to show here the different behaviours of the two approaches in a case for which with the first dynamics we assist to an example of the aforementioned violations of the constraints. In figure 4.27 we can see the full density profiles at different times with control parameters set to $\kappa_1 = 1, \kappa_2 = 0.1, \mu = 1.7, \alpha = 1.5, \beta = 0.6$, obtained using the two different dynamics. In figure 4.27a we can see that, when the time is of the order of magnitude of the system size, some densities close to the ejection side of the TASEP start to have values greater than 1. In figure 4.27b, output of the improved code, this problem is not present and the dynamics keep satisfying the physical constraints during its full evolution. In figure 4.28 we can extract the same information but now from the point of view of the reservoir densities. We see that the density of the second reservoir, theoretically bound to be less than one, exceeds this value when using the incorrect dynamics, while remaining below the threshold while using the correct one. We can also see that, as we pointed out before, the two dynamics are converging on the same stationary values, albeit we are cutting off the plot to better show the different transient behaviours that interested us in this discussion.

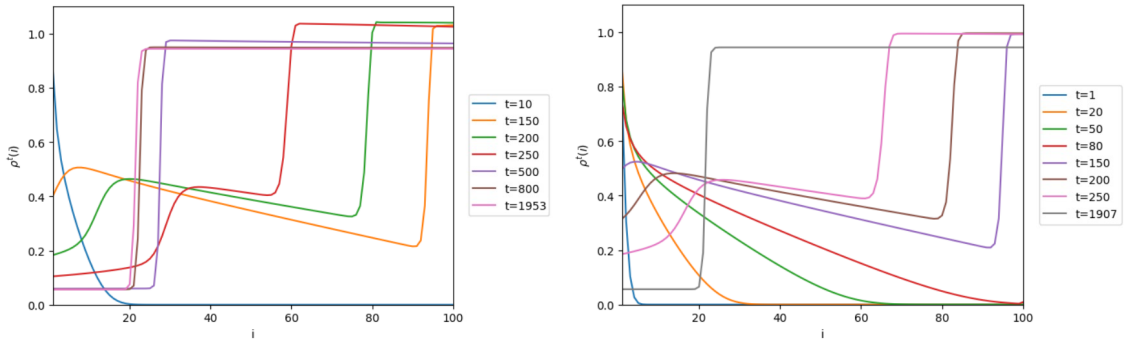

(a) We can see that, for certain times, a portion of the profile density exceeds 1, which is not physically possible.

(b) We can see that, during the dynamics, the profile density always assumes permitted values.

Figure 4.27: Density profile, at various times, for $\kappa_1 = 1, \kappa_2 = 0.1, \mu = 1.7, \alpha = 1.5, \beta = 0.6$, obtained with the two different codes.

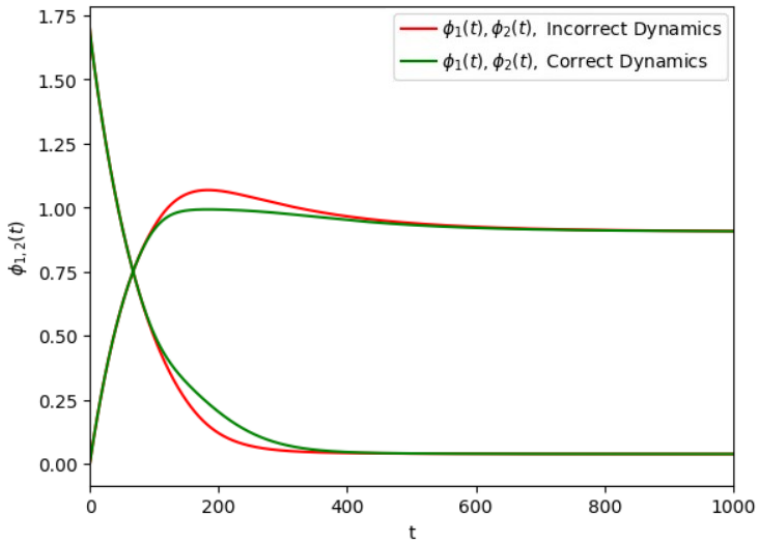

Figure 4.28: Time evolution of the reservoir densities obtained with the two different dynamics proposed. We can see that, for certain times, the incorrect dynamics let $\phi_2(t) > 1$. During the correct dynamics, instead, the constraint $\phi_2(t) < 1$ is always respected.

Chapter 5

Conclusions

In this thesis, we have considered an out-of-equilibrium closed system composed of a TASEP connected to two finite-sized interacting reservoirs. Although these types of models are usually proposed in the statistical physics literature as a modelling tool in various contexts, such as biological transport with finite resources, we have detached from the association to a specific real situation and focused on investigating an idealised system. We have worked out an approximate analytical theory, combined with numerical methods, to investigate how the interplay among a limited number of particles moving in a lattice with non-constant input/output parameters from and to two reservoirs and the process of diffusion between these reservoirs contribute to determining the macroscopic behaviour of the steady state of the aforementioned system. More specifically, the model under investigation is made up of a one-dimensional lattice, whose internal behaviour is that of a TASEP with unitary and uniform transition rates, connected at its end to two reservoirs R_1 and R_2 of different finite capacities that can mutually exchange particles, permitting a non-zero steady state current in the system. The control parameters characterising the model are the entry/exit rates of the TASEP (α, β), the diffusion rates between the reservoirs (k_1, k_2) and the filling factor μ, which gives us information on how populated the total system is, in relation to the size of the lattice. Moreover, we decide to make the injection/extraction processes reservoir population-dependent by defining the effective rates $\alpha_{EFF} = \alpha\frac{N_1}{L}, \beta_{EFF} = \beta(1 - \frac{N_2}{L})$, where L is the size of the TASEP and $N_{1,2}$ represent the number of particles present in $R_{1,2}$, at any given moment. This adjustment is meant to represent the idea that the injection (extraction) process can be facilitated (hindered) by a larger number of particles present in R_1 (R_2). We have used a mixture of both analytical and numerical tools (mean field theory and Kinetic Monte Carlo simulations), to obtain results concerning the Weak Coupling limit of the model. In this limit, the diffusion mechanism between the reservoirs and particle hopping inside the TASEP are comparable. This can be guaranteed by the following scaling for the diffusion rates $k_{1,2} = \frac{\kappa_{1,2}}{L}$, with $\kappa_1, \kappa_2 \sim O(1)$. The situation in which the diffusion overwhelms the TASEP

current is called the Strong Coupling limit. The choice of focusing our analysis on the former scenario was due to the latter one being deemed less interesting and already thoroughly treated in [17]. In the same article, the authors suggest instead the Weak Coupling limit to give rise to an interesting steady state landscape, but the results they present show some unexpected disagreements between theory and simulations and suggested the need for a deeper analysis.

Concerning the results of this thesis work, we have been able to produce phase diagrams representing the steady state behaviour of the system, given any possible combination of the five control parameters listed before, in a Weak Coupling limit, while also obtaining a mean field approximation of the bulk particle densities and steady state reservoir densities. Firstly, we found the critical condition $\kappa_2 = 0.25$ that divides the phase space into two different regions where a Max Current Phase can or cannot be present. We then obtained what seems to be a complete physical landscape in the case $\kappa_2 < 0.25$ where we have seen how, depending upon the value of μ, the model can either be in two or three phases, as shown in the example of figure 4.3. Then we moved to examine the more complicated situation for $\kappa_2 > 0.25$ where we were able to see how, depending upon the value of μ, the model can be in two, three or four phases and we distinguished the existence of at least three different families of behaviours in μ depending on whether the ratio $\frac{\kappa_2}{\kappa_1}$ is smaller, equal or greater than 1. The threshold values of μ for the existence of the various phases have been identified. During this analysis, we also noted that the model admits a particle-hole symmetry for $\kappa_1 = \kappa_2$ and we showed how this symmetry reverberates from the equations to the phase diagrams. We must stress again the fact that all these results have not been proven exactly but obtained in a mean field approximation. However, they have been fully backed quantitatively by the corresponding Kinetic Monte Carlo results. This convincingly suggests that despite the necessary limitations of a mean field approach, most of the relevant physics can be nonetheless contained in this simplified description. Finally, we were able to obtain the full dynamics behaviour of both the particle densities and the reservoir densities in mean field, which can lead to a detailed description of the system's evolution towards stationarity.

Before ending this section, let us list some lines of investigation that we deem worth pursuing as a continuation of this thesis project. First of all, we have mentioned before that a topologically interesting situation arises for certain combinations of the control parameters for which there seem to be separate High Density regions in the (α, β) phase diagrams, following the splitting into two branches of the parametric line that separates this phase and the Domain Wall one. Evidently, one would like to come to a physical understanding of exactly when, in terms of the control parameters, and why this situation could appear. Also, it is natural to wonder whether a symmetric situation can be present for the Low Density phase and whether this may depend on the control parameters. Following these considerations, one should read the diagrams in figure 4.4 as a first draft that, while surely

containing relevant information for the steady state landscape of the model, could probably be improved with other lines indicating some sort of dynamical transitions within the different regions that in this work we have not been able to see. Another important deep dive could be made in terms of analysis of the full dynamics to stationarity in mean field. While we collected all the data, it would be interesting to make a more specific examination of the relaxation towards the steady state, considering the time and way in which these different states are reached and how the control parameters quantitatively influence the relevant variables that can describe this process, like the shock velocities, the relaxation time, and many others. Lastly, we think that there are some slight modifications that can be performed on the system we studied in this work to which our MFT and KMC analysis can be easily extended which would be interesting to consider. The first that comes to mind is to have more than one TASEP connecting two or more reservoirs with the same type of diffusion mechanism. Secondly, one could reconsider the choice of the effective rates $\alpha_{EFF}, \beta_{EFF}$. For these rates, we considered specific functions of the numbers of particles in the reservoirs to obtain the population-dependent behaviour we wanted for the injection and extraction mechanisms. One could expect that by changing those specific functions while maintaining the characteristics to be respectively monotonically increasing and decreasing in their arguments and fixing the finite size of the reservoirs, some qualitatively similar results to the one obtained in this work should hold. Ultimately, in the present work, we considered a TASEP channel with unitary and uniform transition rates and without disorder. One or more of these assumptions could be relaxed in considering more complicated internal lattice dynamics while maintaining the same two reservoirs, injection/extraction effective parameters and diffusion mechanism.

References

[1] C. T. MacDonald, J. H. Gibbs, and A. C. Pipkin. Kinetics of biopolymerization on nucleic acid templates. *Biopolymers 6*, pages 1–5, 1968.

[2] Nicholas H Barton, Derek Briggs, Jonathan Eisen, David Goldstein, and Nipam Patel. *Evolution*. Cold Spring Harbor Laboratory Press, 2007.

[3] D. A. Adams, B. Schmittmann, and R. K. P. Zia. Far from equilibrium transport with constrained resources. *J. Stat. Mech*, 2008.

[4] C. A. Brackley, M. C. Romano, C. Grebogi, and M. Thiel. Limited resources in a driven diffusion process. *Phys. Rev. Lett. 105*, 2010.

[5] C. A. Brackley, M. C. Romano, and M. Thiel. Slow sites in an exclusion process with limited resources. *Phys. Rev. E 82*, 2010.

[6] L. Jonathan Cook and R. K. P. Zia. Feedback and fluctuations in a totally asymmetric simple exclusion process with finite resources. *J. Stat. Mech.: Theory Exp 2009*, 2009.

[7] A. Haldar, P. Roy, and A. Basu. Asymmetric exclusion processes with fixed resources: Reservoir crowding and steady states. *Phys. Rev. E 104*, 2021.

[8] T. Sasamoto. One-dimensional partially asymmetric simple exclusion process with open boundaries: orthogonal polynomials approach. *Journal of Physics A: Mathematical and General*, 1999.

[9] A. Parmeggiani, T. Franosch, and E. Frey. Phase coexistence in driven one-dimensional transport. *Phys. Rev. Lett. 90*, 2003.

[10] L.B. Shaw, R.K.P. Zia, and K.H. Lee. The totally asymmetric exclusion process with extended objects, a model for protein synthesis. *Phys. Rev. E 68*, 2003.

[11] T. Chou and G. Lakatos. Clustered bottlenecks in mrna translation and protein synthesis. *Phys. Rev. Lett. 93*, 2004.

[12] V. B. Priezzhev. Exact nonstationary probabilities in the asymmetric exclusion process on a ring. *Physical Review Letters, 91*, 2003.

[13] B. Derrida, E. Domany, and D. Mukamel. An exact solution of the one dimensional asymmetric exclusion model with open boundaries. *J. Stat. Phys. 69*, pages 667–687, 1992.

[14] B. Derrida, M.R. Evans, V. Hakim, and V. Pasquier. Exact results for the one dimensional exclusion model. *Physica A200*, pages 25–33, 1993.

[15] B. Derrida, M.R. Evans, V. Hakim, and V. Pasquier. A matrix method of solving an asymmetric exclusion model with open boundaries. *Cellular Automata and Cooperative systems*, pages 121–133, 1993.

[16] B. Derrida, S.A. Janowsky, J.L. Lebowitz, and E.R. Speer. Exact solution of the totally asymmetric simple exclusion process: shock profiles. *J. Stat. Phys. 73*, pages 813–842, 1993.

[17] S. Pal, P. Roy, and A. Basu. Availability, storage capacity, and diffusion: Stationary states of an asymmetric exclusion process connected to two reservoirs. *Preprint - arXiv:2308.08384v1*, 2023.

[18] D. T. Gillespie. Exact stochastic simulation of coupled chemical-reactions. *J. Phys. Chem. 81, 2340*, 1977.